INSTRUMENTATION TO MEASURE THE BACKSCATTERING COEFFICIENT b_b FOR ARBITRARY PHASE FUNCTIONS

A Dissertation

by

DAVID HAUBRICH

Submitted to the Office of Graduate Studies of
Texas A&M University
in partial fulfillment of the requirements for the degree of

DOCTOR OF PHILOSOPHY

August 2010

Major Subject: Physics

INSTRUMENTATION TO MEASURE THE BACKSCATTERING COEFFICIENT b_b FOR ARBITRARY PHASE FUNCTIONS

A Dissertation

by

DAVID HAUBRICH

Submitted to the Office of Graduate Studies of
Texas A&M University
in partial fulfillment of the requirements for the degree of

DOCTOR OF PHILOSOPHY

Approved by:

Chair of Committee,	Edward S. Fry
Committee Members,	John W. Bevan
	George W. Kattawar
	George R. Welch
Head of Department,	Edward S. Fry

August 2010

Major Subject: Physics

ABSTRACT

Instrumentation to Measure the Backscattering Coefficient b_b for Arbitrary Phase Functions. (August 2010)

David Haubrich, B.S., Johannes Gutenberg-Universität Mainz

Chair of Advisory Committee: Dr. Edward S. Fry

The backscattering coefficient b_b is one of the inherent optical properties of natural waters which means that it is independent of the ambient light field in the water. As such, it plays a central role in many problems of optical oceanography and is used in the characterization of natural waters. Essentially, any measurement that involves sending a beam of light into water must account for all inherent backscattering. Some of the applications that rely on the precise knowledge of the backscattering coefficient include studies of suspended particle distributions, optical bathymetry, and remote sensing. Many sources contribute to the backscattering, among them any suspended particles, air bubbles, and the water molecules themselves. Due to the importance of precise measurements and the ease with which water samples can be contaminated, an instrument to determine directly and quickly the backscattering coefficient *in situ* is highly desirable.

We present such an instrument in both theory and experiment. We explain the theory behind our instrument and based on measurements made in the laboratory we demonstrate that our prototype shows the predicted behavior. We present data for increased extinction in the water, and show how measuring the extinction and taking it into account improves the quality of our measurements. We present calibration data obtained from three different particle sizes representing differently shaped volume scattering functions. Based on these measurements we demonstrate that our prototype has the necessary resolution to measure the backscattering coefficient b_b

over the whole range found in natural waters. We discuss potential improvements that should be made for a commercial version of the instrument.

TABLE OF CONTENTS

CHAPTER Page

LIST OF TABLES

LIST OF FIGURES

FIGURE Page

CHAPTER I

INTRODUCTION

Water and light are two of the main ingredients for life on earth. Despite their abundance, it was not until the early 1800s that mankind's research into optical oceanography began. Otto von Kotzebue is believed to be the first person to conduct optical oceanographic research during his Rurik circumnavigational cruise in 1817 [1]. Using a piece of red cloth tied to a rope he roughly measured the penetration depth of light. Over the course of the next decades this method was refined, cumulating in the measurements of Secchi [2]. In 1885, photographic methods were first used by Fol and Sarasin, who submerged photographic plates in the Mediterreanean.

The first person to develop and publish a theoretical treatment for marine light scattering was Ludwig Valentin Lorenz in 1890 [3]. Gustav Mie did further work on this theory and presented what today is known as Mie-Theory, sometimes also referred to as Lorenz-Mie Theory in 1908 [4]. This theory uses Maxwell's equations and gives a complete analytical solution for the scattering of electromagnetic radiation on spherical particles; however, it was not widely used until the advent of computers due to the complexity of the calculations.

In the 1950s and 1960s, new instruments and measurements of scattering in water were done by several groups, among them Tyler and Richardson [5] and Kullenberg [6]. Special mention has to be given to the measurements of Petzold [7], whose data is widely used in the description of natural waters today.

Further research led to the development of the wide range of instruments that are now commercially available to measure diverse parameters of natural waters; however,

---

This dissertation follows the style and format of Applied Optics.

a complete discussion of all available instruments for all the different parameters is outside the purview of this work. We will concentrate on backscattering in water, since our instrument was designed specifically for this purpose.

Backscattering plays a central role in many problems of optical oceanography and is used in the characterization of natural waters. Essentially, any measurement that involves sending a beam of light into water has to account for the backscattering that occurs. Some of the applications that rely on the precise knowledge of the backscattering coefficient include studies in suspended particle distributions, optical bathymetry, and remote sensing. Sources contributing to the backscattering include the water molecules themselves, suspended organic and inorganic particulates, and air bubbles.

From a physicist's point of view, the importance of the backscattering coefficient is not based on its rather arbitrary portion of the total scattering coefficient, instead it is founded in the history of optical oceanography. In this discipline, the backscattering coefficient b_b became an important parameter that is used to characterize natural waters and is also used in many equations to connect the inherent optical properties to the apparent optical properties. Some of these relationships will be discussed in Chapter II. Chapter III will briefly review methods currently used to determine the backscattering coefficient and discuss the (dis-)advantages of the methods they use. The thory and design of the instrument is presented in Chapter IV, followed by a description of the experimental setup in Chapter V, and the results in Chapter VI. As is summarized in Chapter VII, the importance of precise measurements and the ease with which water samples can be contaminated make an instrument to directly and quickly determine the backscattering coefficient *in situ* highly desirable.

CHAPTER II

BACKGROUND

It is important to understand that the optical properties that will be discussed in this dissertation are bulk properties of water, and are not meant to be applied on a molecular level. Bulk properties are best determined directly in the open water; apparent optical properties (AOP's) can only be measured *in situ*.

Scattering and absorption are the two fundamental processes involved in the distribution of light in water. These processes give rise to two fundamental IOP's, the volume scattering function and the absorption coefficient. Several other IOP's can be derived once these two are known. These properties are called "inherent", because they are independent of the ambient light field, and thus depend only on the constituents of the water. This fact also allows for the IOP's to be - at least in principle - measured both *in situ* and in the laboratory. Since our instrument has been designed to measure one of these IOP's, we will discuss them in detail in Section A.

In Section B we will briefly discuss AOP's, which will also include defining some general quantities that can be encountered frequently in studies of natural waters. While AOP's are not fundamental, they were the first to be defined and measured. This is because historically, observations were first made using naturally available light sources, usually the sun. Because of this, the AOP's not only depend on the water and its constituents, but also on the ambient light field.

A. Inherent Optical Properties

As mentioned above, the volume scattering function (VSF) $\beta(\lambda, \theta, \phi)$ and the absorption coefficient $a(\lambda)$ are two fundamental IOP's. Other IOP's include the index

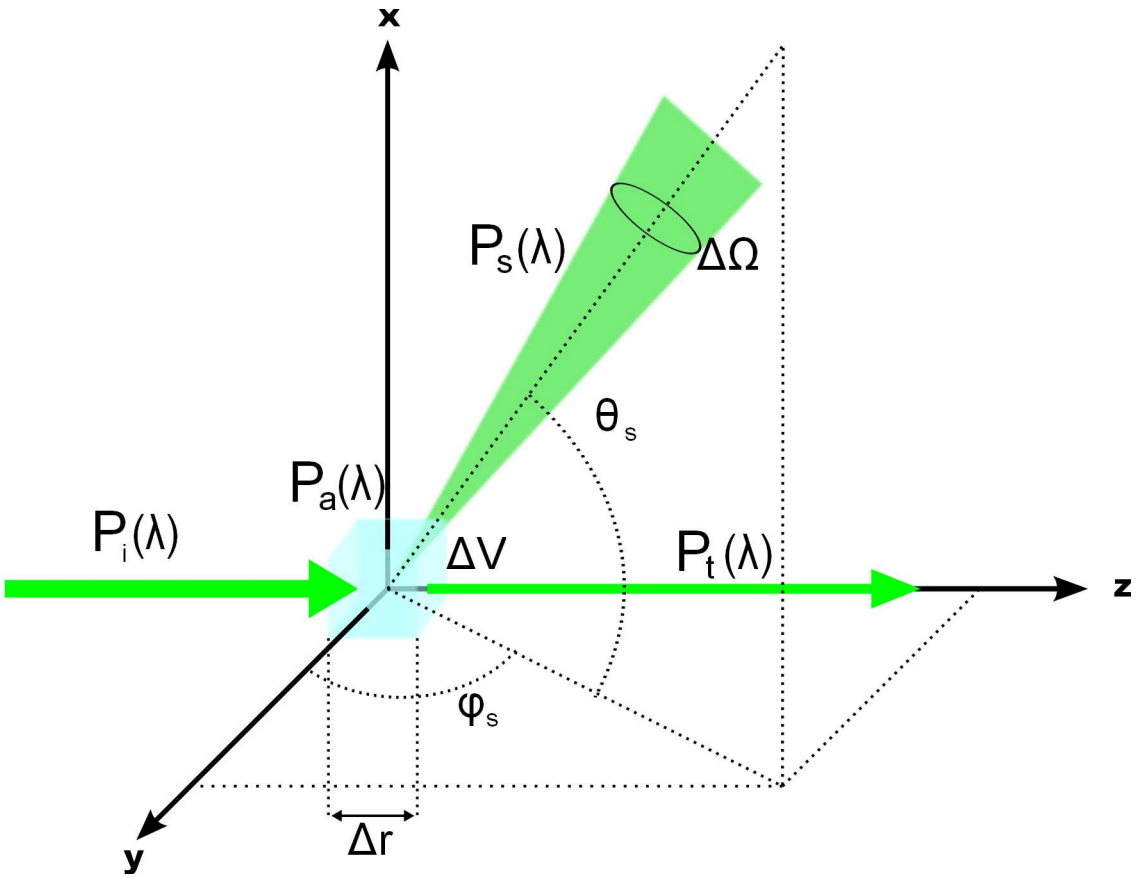

Fig. 1. The interaction between light and matter

of refraction n, the single scattering albedo ω_0, and the total, forward, and back scattering coefficients $b(\lambda)$, $b_f(\lambda)$, and $b_b(\lambda)$, which can all be derived from the two fundamental ones.

In order to define the inherent optical properties, consider a small volume ΔV with thickness Δr (see Fig. 1). We illuminate this volume with a small collimated beam with wavelength λ and incident power $P_i(\lambda)$. Further we define $P_a(\lambda)$, $P_s(\lambda)$, and $P_t(\lambda)$ to be the absorbed, scattered, and transmitted power, respectively. From the energy conservation principle it is obvious that the sum of the absorbed, in all direction scattered, and transmitted power has to be equal to the incident power:

$$P_i(\lambda) = P(\lambda)_a + P(\lambda)_{s,4\pi} + P(\lambda)_t. \tag{2.1}$$

We can now define the dimensionless absorptance $A(\lambda)$, scatterance $B(\lambda)$, and transmittance $T(\lambda)$ as the ratios of the absorbed, scattered, and transmitted powers to the incident power:

$$A(\lambda) = \frac{P(\lambda)_a}{P(\lambda)_i} \tag{2.2}$$

$$B(\lambda) = \frac{P(\lambda)_{s,4\pi}}{P(\lambda)_i} \tag{2.3}$$

$$T(\lambda) = \frac{P(\lambda)_t}{P(\lambda)_i} \tag{2.4}$$

Plugging Eqs.(2.2 - 2.4) into Eq.(2.1) it is easy to see that

$$A(\lambda) + B(\lambda) + T(\lambda) = 1\,. \tag{2.5}$$

The commonly encountered quantities in optical oceanography are the absorption and scattering coefficients, which are defined as the absorptance and scatterance per unit length

$$a(\lambda) \equiv \lim_{\Delta r \to 0} \frac{A(\lambda)}{dr} \tag{2.6}$$

$$b(\lambda) \equiv \lim_{\Delta r \to 0} \frac{B(\lambda)}{dr}\,, \tag{2.7}$$

respectively. The typical unit for these coefficients is m^{-1}, although cm^{-1} is also used.

Frequently, the quantity we are interested in is how much power is lost in the transmission of a beam, irrespective of whether this is due to absorption or scattering. Therefore, we define the beam attenuation coefficient c as the sum of the absorption and scattering coefficients,

$$c(\lambda) \equiv a(\lambda) + b(\lambda)\,. \tag{2.8}$$

Now we can use these coefficients to determine how much power is lost in a light beam propagating in a medium with absorption a, scattering b, or extinction c. The initial power $P(x = 0)$ decreases exponentially with the distance traveled through that medium, thus at a distance x the remaining power $P(x)$ can be calculated by

$$P(x) = P(x = 0) \cdot e^{-(a,b,c)x} \,. \tag{2.9}$$

So far we have only considered the total scattered power, i.e. the power which is scattered in all directions. Taking into account the angular distribution, we define the volume scattering function (VSF)

$$\beta(\lambda, \theta, \varphi) \equiv \lim_{\Delta r \to 0} \lim_{\Delta\Omega \to 0} \frac{B(\lambda, \theta, \varphi)}{\Delta r \Delta\Omega} \tag{2.10}$$

where $B(\lambda, \theta, \varphi)$ is the fraction of the incident power scattered into a solid angle $\Delta\Omega$ centered on (θ, φ). The unit for the VSF is $m^{-1}sr^{-1}$.

From a physicist's point of view we also can interpret the volume scattering function as the differential scattering cross section per unit volume. Looking at the definition of $\beta(\lambda, \theta, \varphi)$ it is clear that integration of the volume scattering function over all solid angles gives the total scattering coefficient $b(\lambda)$. We can therefore write

$$b(\lambda) = \int_{4\pi} \beta(\lambda, \theta, \varphi) d\Omega = 2\pi \int_{0}^{\pi} \beta(\lambda, \theta) \sin\theta d\theta. \tag{2.11}$$

We are able to do the integration over φ because for natural waters the scattering is azimuthally symmetric about the incident direction, as long as we assume that the scatterers are randomly oriented. Furthermore, it is useful to separate the integration in Eq. (2.11) into the forward scattering, $0 \leqslant \theta \leqslant \pi/2$, and the backward scattering, $\pi/2 \leqslant \theta \leqslant \pi$, parts, and to define the forward and backward scattering coefficients,

b_f and b_b, respectively, as

$$b_f(\lambda) \equiv 2\pi \int_0^{\pi/2} \beta(\lambda, \theta) \sin\theta d\theta \tag{2.12}$$

$$b_b(\lambda) \equiv 2\pi \int_{\pi/2}^{\pi} \beta(\lambda, \theta) \sin\theta d\theta \, . \tag{2.13}$$

From the VSF and these coefficients, we can derive three other frequently encountered quantities. These are, while not fundamental, quite useful in describing and comparing natural waters. The first of these quantities is the volume scattering phase function $\tilde{\beta}(\lambda, \theta)$, often shortened to "phase function". It is defined as the VSF divided by the total scattering coefficient:

$$\tilde{\beta}(\lambda, \theta) \equiv \frac{\beta(\lambda, \theta)}{b(\lambda)} \tag{2.14}$$

Combining this expression with Eq. (2.11) we see that the phase function is normalized to

$$\int_{4\pi} \tilde{\beta}(\lambda, \theta) d\Omega = 1. \tag{2.15}$$

This normalization effectively separates the shape of the volume scattering function from the total strength of the scattering. As such, it is particularly useful to compare the shape of different volume scattering functions, irrespective of the absolute magnitude of the scattering.

The single-scattering albedo is defined as

$$\omega_0(\lambda) \equiv \frac{b(\lambda)}{c(\lambda)}. \tag{2.16}$$

Thus, the value range for the single-scattering albedo is $0 \leqslant \omega_0(\lambda) \leqslant 1$, where values

of 0 and 1 indicate beam attenuation due to absorption and scattering, respectively.

The asymmetry parameter is defined as the average over all scattering directions of the cosine of the scattering angle θ:

$$g \equiv 2\pi \int_0^\pi \tilde{\beta}(\lambda, \theta) \cos\theta \sin\theta d\theta \tag{2.17}$$

It is a measure of the symmetry of the phase function, with values of g near 1 and -1 for strongly forward/backward peaked phase functions, respectively, i.e. $\tilde{\beta}(\lambda, \theta)$ is large/small for small θ and small/large, often by several orders of magnitude, for θ near $180\,^\circ$. For a totally symmetric phase function about $\theta = 90\,^\circ$ the asymmetry parameter takes on a value of 0.

The volume scattering function and the absorption coefficient are generally considered to be fundamental IOP's; others can be derived from these two. Knowledge of those two quantities provides a description of the optical properties of a body of water with regard to the underwater light field using radiative transfer theory.

Both scattering and absorption are independent of the ambient light field and, in principle, water samples can be taken *in situ* and then analyzed in the laboratory. An instrument that can measure these quantities *in situ* is preferable, however, for reasons including the extreme difficulties involved in keeping the sample clean from contaminants, and the problem of the rapid disintegration of the majority of particulate matter which is of organic nature. Thus far, we have explicitly written the wavelength dependence of all optical properties into their definitions. In order to increase the readability of equations, from now on the λ will be omitted from the list

of dependent variables, except where necessary, i.e.

$$b_b \equiv b_b(\lambda)$$

$$\beta(\theta) \equiv \beta(\lambda, \theta)$$

$$etc;$$

however, it must be understood that the wavelength dependence of these values is implied.

B. Apparent Optical Properties

Some properties of bodies of water do not fall into the category of the inherent optical properties; while these are not fundamental, they are generally easier to measure and thus are often used to describe natural waters.

Unlike the IOP's, the AOP's depend not only on the properties of the medium but also on the directional structure of the ambient light field. Due to this dependence it is impossible to determine AOP's through sample measurements in laboratory environments. Using radiative transfer theory, AOP's can be related to IOP's. Before we can show examples of AOP's, we want to present the following definitions. While some of the following quantities might be deemed trivial or generally known by the reader, we consider them important enough to give their definitions in order to prevent any possible misunderstandings.

First, we want to define several quantities and equations directly related to the distribution of light.

The radiant flux F is defined as the power P per time t

$$F = \frac{dP}{dt} \tag{2.18}$$

The unit of the radiant flux is Watt [W].

The light intensity at an angle ζ to the incoming beam is defined as the radiant flux through the solid angle d Ω

$$I(\zeta) = \frac{dF(\zeta)}{d\Omega(\zeta)} \tag{2.19}$$

The radiance L is the light intensity I emitted at an angle ζ by an infinitesimally small element dA through the solid angle $dd\Omega$

$$L(\zeta) = \frac{dI(\zeta)}{dA\cos\theta} = \frac{dP}{dA\cos\theta d\Omega dt} \tag{2.20}$$

where θ is the angle between the normal and direction ζ. Its unit is $[W\ m^{-2}\ sr^{-1}]$.

The irradiance E can be defined as

$$E = \int_{4\pi} L(\zeta)\cos\theta d\Omega. \tag{2.21}$$

Commonly, the irradiance is divided into updwelling and downdwelling irradiances, E_u and E_d, where the integration in Eq. (2.21) is taken over the upper and lower hemisphere, respectively.

A widely used example for an apparent optical property is the irradiance reflectance R_D, defined as

$$R_D = \frac{E_u}{E_d}, \tag{2.22}$$

The irradiance reflectance is also known as "diffuse reflectance". Another frequently encountered pair of AOP's are the diffuse attenuation coefficients of updwelling and downdwelling light in the water, K_u and K_d, respectively:

$$K_u = -\tfrac{1}{E_u}\tfrac{dE_u}{dz} \tag{2.23}$$

$$K_d = -\tfrac{1}{E_d}\tfrac{dE_d}{dz} \tag{2.24}$$

In order for such a quantity to be a useful description of the body of water the quantity must meet certain requirements: on one hand it has to be descriptive enough to differ between two different bodies of water and on the other hand it should be relatively insensitive to environmental factors such as cloud cover or sea state. Consider, for example, an irradiance, which can change by orders of magnitude very quickly if a cloud covers the sun temporarily, or if the surface of the water becomes distorted by waves. As such, the irradiance is not a very useful quantity. However, looking at ratios of irradiances and their rate of change with depth, it is found that these ratios are fairly independent of environmental factors and can therefore be used as descriptive properties of bodies of water.

C. Scattering Theory

1. Rayleigh Theory

Lord Rayleigh's theory of the scattering dipole, published in 1871 [8, 9], was the first explanation for light scattering. In 1899 [10] Rayleigh made the assumption that the molecules themselves formed the dipoles. His approach requires the particles to be small compared to the wavelength of the scattered light. In 1920 Rayleigh [11] and Cabannes [12] modified the theory to include the anisotropy of molecules. While this approach works well for gases, it does not satisfactorily apply to dense media like liquids. Despite this, because several valid results can be obtained from Rayleigh's scattering theory, we will introduce it first before delving into the fluctuation theory by Smoluchowski and Einstein.

If an arbitrarily shaped particle with polarizability p is placed in an electric field $\mathbf{E}$, it can be treated as a dipole, in which a dipole moment

$$\mathbf{P} = p\mathbf{E} \tag{2.25}$$

is induced. Scattering is then explained as a result of the oscillation caused by the incident radiation. The frequency of this oscillation is determined by the frequency of the incident radiation. The scattered intensity I of a monochromatic, parallel, and unpolarized beam with intensity I_0 incident on an isotropic particle observed at a distance R at an angle θ is given as

$$I(\theta) = I_0 \frac{1 + cos^2\theta}{2R^2} \left(\frac{2\pi}{\lambda}\right)^4 p^2. \tag{2.26}$$

Replacing the polarizability p in the previous equation using the Lorentz-Lorenz equation for isotropic, spherical particles with diameter d and refractive index n,

$$p = \frac{n^2 - 1}{n^2 + 2} \left(\frac{d}{2}\right)^3, \tag{2.27}$$

we can write the Rayleigh scattering function in its most common form

$$I\left(\theta\right) = I_0 \frac{1 + \cos^2\theta}{2R^2} \left(\frac{2\pi}{\lambda}\right)^4 \left(\frac{n^2 - 1}{n^2 + 2}\right)^2 \left(\frac{d}{2}\right)^6. \tag{2.28}$$

This equation is often expressed in terms of the dimensionless size parameter X,

$$X = \frac{2\pi r}{\lambda}, \tag{2.29}$$

where r is the radius of the particle and λ the wavelength of the incident light ($r \ll \lambda$). Thus we can rewrite Eq. (2.28) as

$$I\left(\theta\right) = I_0 \frac{1 + \cos^2\theta}{2R^2} X^4 \left(\frac{n^2 - 1}{n^2 + 2}\right)^2 \left(\frac{d}{2}\right)^2. \tag{2.30}$$

Two important results can directly be seen from this equation: Firstly, the wavelength dependence of the scattering on $\frac{1}{\lambda^4}$ and secondly, the symmetry around $90\,^\circ$ of the scattering intensity. The latter is clearly visible in Fig. 2.

Considering the intensities scattered by the particles to be additive, one can express the scattering coefficient b of a unit volume containing N spherical particles.

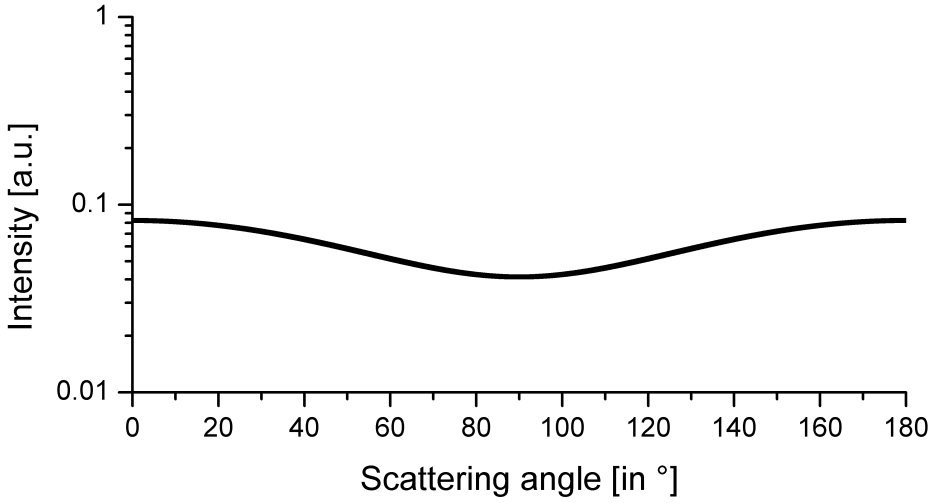

Fig. 2. Rayleigh scattering phase function

Define the Rayleigh ratio $\Re$ as

$$\Re = N\frac{I_{90}}{I_0}R^2 = N\frac{8\pi^4}{\lambda^4}p^2. \tag{2.31}$$

Note that the Rayleigh ratio is the same as the volume scattering function at $90\,^\circ$,

$$\Re = \beta_{90}. \tag{2.32}$$

Combining Eq. (2.28) with Eqs. (2.31) and (2.32) one obtains a simple expression for $\beta(\theta)$,

$$\beta\left(\theta\right) = \beta_{90}\left(1+\cos^2\theta\right). \tag{2.33}$$

Integrating this equation over 4π to get the total scattering coefficient b we find

$$b = \int_0^{2\pi} d\phi \int_0^{\pi} \beta_{90}\left(1+\cos^2\theta\right)\sin\theta d\theta = \frac{16\pi}{3}\beta_{90}. \tag{2.34}$$

Using the Lorentz-Lorenz formula in Eq. (2.27), we can rewrite Eq. (2.31) as

$$\Re = N\frac{8\pi^4}{\lambda^4}\left(\frac{n^2-1}{n^2+2}\right)^2\left(\frac{d}{2}\right)^6, \tag{2.35}$$

where d is the diameter of the scattering particle. Combining the last two equations, we get

$$b = \frac{16\pi}{3}8N\left(\frac{\pi}{\lambda}\right)^4\left(\frac{n^2-1}{n^2+2}\right)^2\left(\frac{d}{2}\right)^6. \tag{2.36}$$

In 1918, Strutt [13] experimentally demonstrated a slight deviation of the polarization from the right angle, which was explained by Rayleigh in 1920 [11] as depolarization by anisotropy of molecules. Rayleigh related the depolarization ratio

$$\delta = \frac{i_2(90)}{i_1(90)} \tag{2.37}$$

to the three components of the polarizability vector. In the same year Cabannes [12] reported what he called the total Rayleigh ratio $\Re_{tot}$ as

$$\Re_{tot} = \Re_{iso}\frac{6+6\delta}{6-7\delta}, \tag{2.38}$$

where $\Re_{iso}$ is given by Eq. (2.35). Consequently, Eqs. (2.33) and (2.34) need to be modified to read

$$\beta(\theta) = \beta(90)\left(1+\frac{1-\delta}{1+\delta}\cos^2\theta\right) \tag{2.39}$$

and

$$b = \frac{8\pi}{3}\beta(90)\frac{2+\delta}{1+\delta}, \tag{2.40}$$

respectively.

We previously noted that for this theory to be applicable, there is a size restriction of the particle size compared to the wavelength. This limit stems from the assumption made in the derivation of Eq. (2.28) that the electric field is homogeneous across the dipole. To assure this, the particle has to be significantly smaller than the wavelength.

This requirement can be expressed in terms of the size parameter X (see Eq (2.29)). The size limit of the particle is then

$$X \ll 1. \tag{2.41}$$

2. Fluctuation Theory

A completely different theory of how light scatters in dense media was presented by Smoluchowski [14] and Einstein [15]. Their approach was based on statistical thermodynamics, since they initially wanted to explain the phenomenon of critical opalescence. They found that their theory not only applied to large density fluctuations that caused critical opalescence, but also could be applied to small density fluctuations and thus explain scattering in liquids.

While the wavelength dependence and general symmetry of the volume scattering function obtained by Rayleigh holds true for dense media as well, we will obtain a different expression for the isotropic part of the Rayleigh ratio, $\Re_{iso}$. Einstein and Smoluchowski considered scattering as an effect caused by the random motion of molecules. In a sufficiently small volume element ΔV this motion will cause density fluctuations $\Delta\rho$, which in turn will lead to small changes in the dielectric constant ϵ. We can relate the mean squares of these fluctuations, $\langle\overline{\Delta\epsilon}\rangle^2$ and $\langle\overline{\Delta\rho}\rangle^2$, as follows:

$$\langle\overline{\Delta\epsilon}\rangle^2 = \left(\frac{d\epsilon}{d\rho}\right)^2 \langle\overline{\Delta\rho}\rangle^2. \tag{2.42}$$

The Rayleigh ratio is given in this theory by

$$\Re_{iso} = \frac{\pi^2}{2\lambda_0^4}\Delta V\langle\overline{\Delta\epsilon}\rangle^2, \tag{2.43}$$

where λ_0 is the wavelength of the incident beam *in vacuo*. Combining the last two

equations we get

$$\Re_{iso} = \frac{\pi^2}{2\lambda_0^4}\Delta V \left(\frac{d\epsilon}{d\rho}\right)^2 \langle\overline{\Delta\rho}\rangle^2. \tag{2.44}$$

The following relation can be found from statistical thermodynamics:

$$\Delta V \left(\frac{d\epsilon}{d\rho}\right)^2 = k_B T \beta_T \rho^2, \tag{2.45}$$

where k_B is the Boltzmann constant, T the absolute temperature, and β_T the isothermal compressibility. Using the simple relationship between the dielectric constant ϵ and the index of refraction n

$$n = \sqrt{\epsilon} \tag{2.46}$$

we get

$$\Re_{iso} = \frac{2\pi^2}{\lambda_0^4} k_B T \beta_T \rho^2 \left(n\frac{dn}{d\rho}\right)^2. \tag{2.47}$$

The difficulty now becomes to find a suitable expression of $dn/d\rho$. Several empirical theoretical equations have been proposed, Einstein [15] for example, used that of Lorentz-Lorenz

$$\frac{n^2-1}{n^2+2}\frac{1}{\rho} = const, \tag{2.48}$$

which leads to his expression of the Rayleigh ratio

$$\Re_{iso} = \frac{\pi^2}{2\lambda_0^4} k_B T \beta_T \frac{\left(n^2-1\right)^2\left(n^2+2\right)^2}{9}. \tag{2.49}$$

King [16] and Rocard [17] suggested using the Sellmeier formula $(n^2-1)/\rho = const.$, and the Gladstone-Dale formula $(n-1)/\rho = const.$. The main problem common to all these equations, however, is that the relationship between n and ρ is considered to be independent of pressure and temperature, which experiments have shown to be untrue. Thus, formulae are instead used that include the experimentally determined values for $(\partial n/\partial T)_P$ and $(\partial n/\partial P)_T$. Depending on whether one chooses T or P to describe the thermodynamic state, $d\epsilon/d\rho$ is replaced by one of the partial

derivatives $(\partial\epsilon/\partial P)_T$ or $(\partial\epsilon/\partial T)_P$, respectively. In the first case, we get

$$\rho\frac{d\epsilon}{d\rho} = \frac{1}{\beta_T}\left(\frac{\partial\epsilon}{\partial P}\right)_T = \frac{2n}{\beta_T}\left(\frac{\partial n}{\partial P}\right)_T, \tag{2.50}$$

and thus

$$\Re_{iso} = \frac{2\pi^2}{\lambda_0^4}k_B T n^2 \frac{1}{\beta_T}\left(\frac{\partial n}{\partial P}\right)_T^2. \tag{2.51}$$

In the latter case we get

$$\rho\frac{d\epsilon}{d\rho} = -\frac{1}{\alpha_P}\left(\frac{\partial\epsilon}{\partial T}\right)_P = -\frac{2n}{\alpha_P}\left(\frac{\partial n}{\partial T}\right)_P, \tag{2.52}$$

obtaining

$$\Re_{iso} = \frac{2\pi^2}{\lambda_0^4}k_B T n^2 \frac{\beta_T}{\alpha_P}\left(\frac{\partial n}{\partial T}\right)_P^2, \tag{2.53}$$

where α_P is the volume expansion coefficient.

Coumou *et al.* [18] investigated both approaches in 1964 and concluded that Eq. (2.51) is the better approximation due to the fact that the corrective term caused by temperature fluctuations can be neglected. Kratohvil *et al.* [19] and Deželić [20] showed that, particularly in the case of water, complete formulae are useless. Using Eq. (2.51), all that is needed to obtain the isotropic part of the Rayleigh ratio are physical constants and experimentally determined values of β_T and $(\partial n/\partial P)_T$. In the same article ([18]), Coumou *et al.* also showed experimentally that Eq. (2.38) remains valid for liquids. We can therefore combine Eqs. (2.38) and (2.51) to get a final expression for the Rayleigh ratio:

$$\Re_{tot} = \frac{2\pi^2}{\lambda_0^4}k_b T n^2 \frac{1}{\beta_T}\left(\frac{\partial n}{\partial P}\right)_T^2 \frac{6+6\delta}{6-7\delta} \tag{2.54}$$

3. Mie Theory

At the same time as Smoluchowski and Einstein were working on their fluctuation theory, Gustav Mie laid the foundations for rigorous theoretical treatment of absorp-

tion and scattering by small particles [4]. Mie presented an analytical solution for the scattering of electromagnetic radiation by a spherical particle using Maxwell's equations. Previous work on the subject had been done by Lorenz in 1890 [3], thus Mie Theory is also known as Lorenz-Mie Theory. We want to give only a brief summary of Mie Theory, as a complete treatment can be found in many text books on scattering, for example in Bohren and Huffman [21], whose text we will closely follow in this section.

A general formulation of the scattering problem is to determine the electromagnetic field $(\vec{E}, \vec{H})$ at all points in- and outside a particle of given size, shape and index of refraction, which might be embedded in a surrounding homogeneous medium, illuminated by an arbitrarily polarized, monochromatic wave. This electromagnetic field must satisfy the vector wave equation

$$\nabla^2 \vec{E} + k^2 \vec{E} = 0 \quad \nabla^2 \vec{H} + k^2 \vec{H} = 0\,. \tag{2.55}$$

Additional conditions on, and relations between, $\vec{E}$ and $\vec{H}$ are given by the Maxwell equations

$$\nabla \cdot \vec{E} = 0 \tag{2.56}$$

$$\nabla \cdot \vec{H} = 0 \tag{2.57}$$

$$\nabla \times \vec{E} = i\omega\mu\vec{H} \tag{2.58}$$

$$\nabla \times \vec{H} = -\,i\omega\epsilon\vec{E}, \tag{2.59}$$

where $k^2 = \omega^2\epsilon\mu$. The problem of finding $\vec{E}$ and $\vec{H}$ can be reduced to finding a solution ψ to the scalar wave equation,

$$\nabla^2\psi + k^2\psi = 0, \tag{2.60}$$

in the following way: Given a scalar function ψ and an arbitrary vector $\vec{c}$ we can construct a vector function $\vec{M}$ by

$$\vec{M} = \nabla \times (\vec{c}\psi)\,. \tag{2.61}$$

This vector function automatically satisfies the first two Maxwell equations, Eqs. (2.56) and (2.57), since the divergence of the curl of any arbitrary vector $\vec{a}$ is identically zero:

$$\nabla \cdot (\nabla \times \vec{a}) = 0. \tag{2.62}$$

Using the vector identities

$$\nabla \times \left(\vec{A} \times \vec{B}\right) = \vec{A}\left(\nabla \cdot \vec{B}\right) - \vec{B}\left(\nabla \cdot \vec{A}\right) + \left(\vec{B} \cdot \nabla\right)\vec{A} - \left(\vec{A} \cdot \nabla\right)\vec{B}, \tag{2.63}$$

$$\nabla\left(\vec{A} \cdot \vec{B}\right) = \vec{A} \times \left(\nabla \times \vec{B}\right) + \vec{B} \times \left(\nabla \times \vec{A}\right) + \left(\vec{B} \cdot \nabla\right)\vec{A} + \left(\vec{A} \cdot \nabla\right)\vec{B} \tag{2.64}$$

we can rewrite Eq. (2.61) as

$$\nabla^2\vec{M} + k^2\vec{M} = \nabla \times \left[\vec{c}\left(\nabla^2\psi + k^2\psi\right)\right]. \tag{2.65}$$

A second vector function $\vec{N}$ can be constructed from $\vec{M}$ by

$$\vec{N} = \frac{\nabla \times \vec{M}}{k}. \tag{2.66}$$

These two vector functions satisfy all requirements we placed upon the electromagnetic field. Thus we have reduced the problem of finding solutions $(\vec{E}, \vec{H})$ to the vector wave equations to the comparatively easier task of finding a solution ψ for the scalar wave equation.

At this point the geometry of the scatterer determines which form ψ takes. Since we are interested in scattering by spherical particles, we chose to write the scalar wave

equation in spherical polar coordinates,

$$\frac{1}{r^2}\frac{\partial}{\partial r}\left(r^2\frac{\partial\psi}{\partial r}\right)+\frac{1}{r^2\sin\Theta}\frac{\partial\psi}{\partial\Theta}\left(\sin\Theta\frac{\partial\psi}{\partial\Theta}\right)+\frac{1}{r^2\sin\Theta}\frac{\partial^2\psi}{\partial\phi^2}+k^2\psi=0. \tag{2.67}$$

The solutions to this equation can be written as

$$\psi_{emn}=\cos m\phi P_n^m\left(\cos\Theta\right)z_n\left(kr\right), \tag{2.68}$$

$$\psi_{omn}=\sin m\phi P_n^m\left(\cos\Theta\right)z_n\left(kr\right), \tag{2.69}$$

where P_n^m are the associated Legendre functions of the first kind of degree n and order m, and z_n is any of the four spherical Bessel functions

$$j_n(\rho)=\sqrt{\frac{\pi}{2\rho}}J_{n+1/2}(\rho), \tag{2.70}$$

$$y_n(\rho)=\sqrt{\frac{\pi}{2\rho}}Y_{n+1/2}(\rho), \tag{2.71}$$

$$h_n^{(1)}(\rho)=j_n(\rho)+iy_n(\rho),\ \ and \tag{2.72}$$

$$h_n^{(2)}(\rho)=j_n(\rho)-iy_n(\rho). \tag{2.73}$$

Having found a solution to the scalar wave equation we can construct solutions to the vector wave equations:

$$\vec{M}_{emn}=\nabla\times\ \left(\vec{r}\psi_{emn}\right) \tag{2.74}$$

$$\vec{M}_{omn}=\nabla\times\ \left(\vec{r}\psi_{omn}\right) \tag{2.75}$$

$$\vec{N}_{emn}=\frac{\nabla\times\vec{M}_{emn}}{k} \tag{2.76}$$

$$\vec{N}_{omn}=\frac{\nabla\times\vec{M}_{omn}}{k}. \tag{2.77}$$

Thus we have found a way to expand any electromagnetic field in an infinite series of spherical harmonics. It is now possible to use these expansions in addition to boundary conditions to describe the scattering of an electromagnetic field on any

object. The major difficulty becomes in finding a suitable expansion for the field and object. Luckily, this expansion is, while cumbersome, relatively straightforward for scattering on a spherical particle. Additionally, due to the necessity of using recursion relations to calculate the Bessel functions, a large amount of computing power is necessary. Thus, although exact, calculations using Mie theory were not practical until the availability of computers. Today many codes are available for computing scattering functions; two of the most widely used are the code presented by Bohren and Huffman [21] and the one published by Mishchenko *et al.* in the book *Scattering, Absorption, and Emission of Light by Small Particles* [22].

D. Theoretical Backscattering Coefficient of Pure Water

Given the Rayleigh scattering for a single spherical particle with diameter d

$$I = I_0 \frac{1+\cos^2\theta}{2R^2} X^4 \left(\frac{n^2-1}{n^2+2}\right)^2 \left(\frac{d}{2}\right)^2 \quad , \tag{2.78}$$

we can make a "back of the envelope" calculation to get an idea of the backscattering coefficient for pure water. Of course, as we have discussed in Section C, this calculation will not provide us with the exact value. As we will see, however, our result will be close to the value obtained using the fluctuation theory.

Assuming a diameter of an H_2O molecule of $0.275\,nm$, the size parameter at a wavelength of $\lambda = 532\,nm$ is

$$X_{H_2O,532nm} = \frac{2\pi r}{\lambda} = \frac{2\pi \cdot 0.1375\,nm}{532\,nm} \simeq 1.6239 \cdot 10^{-3}\,. \tag{2.79}$$

Since this value is much smaller than 1, it justifies our usage of the Rayleigh scattering theory instead of having to use the more general Mie theory.

We can now find the Rayleigh scattering cross section

$$\sigma_s = \frac{2\pi^5}{3}\frac{d^6}{\lambda^4}\left(\frac{n^2-1}{n^2+2}\right)^2 . \tag{2.80}$$

To obtain the scattering coefficient b for pure water, we have to multiply the scattering cross section with the number of particles per unit volume. Since the standard unit of the scattering coefficient is m^{-1}, we will express the scattering cross section and the unit volume in m^2 and m^3, respectively. Given the molar mass of water of $18.01524\, g\, mol^{-1}$ and its density of $1000\, kg\, m^{-3}$ we find that we need

$$\frac{1000\,\frac{kg}{m^3}}{18.01524\,\frac{g}{mol}} = 55508.55831\, mol\ \ H_2O\, . \tag{2.81}$$

Multiplying this value by Avogadro's number

$$N_A = 6.02214 \cdot 10^{23}\, mol^{-1} \tag{2.82}$$

we get the total number j of H_2O molecules per m^3:

$$j = 55508.55831\, mol \cdot N_A = 3.342801262 \cdot 10^{28} \tag{2.83}$$

Plugging all the values into Eq. (2.80) we find the total scattering coefficient of water at $\lambda = 532\, nm$:

$$b = j\sigma_s = 1.53 \cdot 10^{-3}\, m^{-1}\, . \tag{2.84}$$

Due to the symmetry of Rayleigh scattering we can write that one half of the scattering is forward, the other half backward,

$$\frac{b_b}{b} = \frac{1}{2} \tag{2.85}$$

and therefore we get a value for the backscattering coefficient of pure water based on

Rayleigh theory of

$$b_b(H_2O,\ 532nm) = 7.66 \cdot 10^{-4}\, m^{-1}\ . \tag{2.86}$$

In this calculation, we made two assumptions: first, that the water molecules are spherical, and second, that there are no density fluctuations in the water. In 1974 Morel [23] published the currently accepted value of $b_b = 8.95 \cdot 10^{-4} m^{-1}$ (at 525 nm). In his calculations he included density fluctuations and the real molecular size and shape of the water molecules, but even without those, our quick estimate is, in fact, rather close to Morel's number.

E. Optical Properties of Natural Waters

Now that we have established the theoretical framework for light distribution in natural waters, let us briefly discuss what we have to expect when dealing with natural waters. The term "natural waters" is used to avoid any confusion with the properties of pure water. Unfortunately, the properties of natural waters are very seldom close to those of pure water, due to the plethora of foreign matter in the water that affects both absorption and scattering. One of the difficulties in measuring properties of natural waters arises from the fact that the variety of dissolved and particulate matter components can change the properties by multiple orders of magnitude, thus requiring a large dynamic range of instruments designed to measure these values. The large number of different factors influencing water properties makes it also hard to compare measurements taken at different locations and/or times. Let us look, for example, at the backscattering coefficient b_b. We can write the total backscattering as a sum of the constituent contributions,

$$b_b = b_{b\,pw} + \sum_{i=1}^{N} b_{b\,i} \tag{2.87}$$

where N is the number of different contributors with a backscattering of $b_{b\,i}$. Natural waters consist of particles with a continuous size distribution, which, simplified, can be expressed by the Junge distribution $J(X)$ as

$$J(X) = const \cdot X^{-\xi}\,, \tag{2.88}$$

where ξ is the characteristic parameter for a sample, which for natural waters generally varies from 2.6 to 3.0; and X is the size parameter, defined by Eq. (2.29). It has to be noted, however, that this simple distribution frequently overestimates the number of small ($d \leq 1\,\mu m$) particles while underestimating the number of larger particles. Additionally, spatial and temporal variations exist, for example due to organic growth, that can only be captured by actual measurements.

Historically, particles with sizes smaller than $0.4\,\mu m$ are called dissolved matter, those larger, particulate matter. This rather arbitrary separation has its origin in the filtration of water. Typically the smallest pore sizes were of the order of $0.4\,\mu m$ and thus everything that was caught by the filter was designated as particulate, anything that stayed in the water was called dissolved. Further classification is separation into categories of organic and inorganic, and living and non-living. For a detailed description of the various constituents of natural waters see, for example, Chapter 3 of Curtis D. Mobley's book *Light and Water* [24].

From the measurements of Petzold [7] an averaged volume scattering phase function for natural waters has been defined; this so called Petzold phase function is shown in Fig. 3. As can be seen, the scattering is strongly forward peaked, indicating that the scattering is dominated by particles with a size parameter significantly greater than one, such that Rayleigh theory cannot be applied to obtain even approximate values.

As our instrument is designed to measure the backscattering coefficient, we now

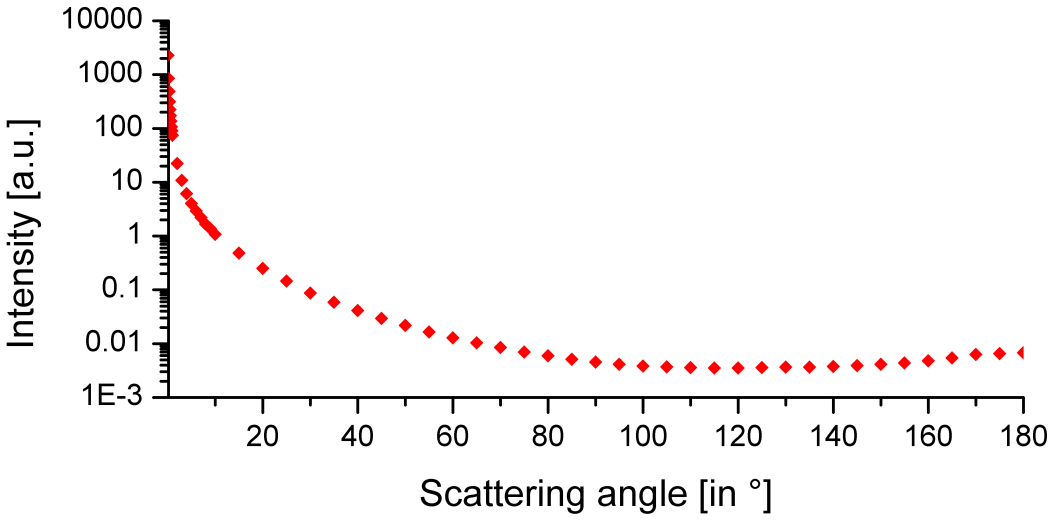

Fig. 3. Petzold phase function

want to look at the range of the backscattering coefficients in various natural waters. Since most measurements have been made at different wavelengths, it is difficult to find easily comparable data. Although our instrument operates at the laser wavelength of $\lambda = 532\,nm$, Table I shows the backscattering coefficient in different types of water at a wavelength of $\lambda = 514\,nm$, as this is the wavelength at which Petzold's VSF meter operated and for which data is more readily available. In addition to b_b obtained from his measurements of the VSF in different waters, Table I contains the value for pure water obtained from Buiteveld *et al.* in 1994 [25] ($b_b/b = 0.5$) and that for pure sea water as reported by Morel [23].

As can be seen from Table I, natural waters have a wide range in the value of the backscattering coefficient, depending on the location where the measurements are taken. Generally, the clearest waters are found in the ocean far from land, while higher values for b_b are found in shallow, turbid waters, where air bubbles may also have a significant influence on the backscattering.

Table I. Approximate results for the backscattering coefficient at $\lambda = 514\,nm$

Type of water	b_b $[m^{-1}]$
Pure water (Buiteveld *et al.* [25])	0.00095
Pure sea water (Morel [23])	0.00125
Clear ocean (Petzold [7])	0.00163
Coastal ocean (Petzold [7])	0.00285
Turbid harbor (Petzold [7])	0.03648

We must keep in mind that with our instrument we will expect slightly lower values, as it operates at a wavelength of $\lambda = 532\,nm$ and the fact that backscattering in natural waters decreases with longer wavelengths.

As will be described in depth in Chapter IV, absorption has a non-negligible effect on our instrument and, therefore, we want to at least mention the range in which it occurs. The expected absolute minimum for the absorption coefficient is given by the absorption of pure water, which has been experimentally determined by Pope and Fry in 1997 [26] to have a value of $a_{pw} = 0.0447\,m^{-1}$ at $\lambda = 532.5\,nm$. Typically, values of a in natural waters range from $0.05\,m^{-1}$ to more than $50\,m^{-1}$.

CHAPTER III

CURRENT INSTRUMENTS

Despite the importance of the knowledge of the backscattering coefficient for a multitude of applications, there have been relatively few successful approaches to measure the backscattering coefficient, in the laboratory or *in situ*. Currently, the methods to determine the backscattering coefficient in both cases are based on one of the following principles:

- A measurement of the volume scattering function (VSF) and calculation of b_b
- An integrating cavity to collect backscattered light
- A fixed-angle ("Magic Angle") backscattering meter
- A measurement of several AOPs and application of an inversion algorithm

We will briefly introduce each of the methods and discuss their respective advantages and disadvantages. It should be noted that, to our knowledge, the only commercially available instruments to directly measure the backscattering coefficient *in situ* are based on the fixed angle approach. The design of instruments measuring the scattering in water is driven by the (exact) mathematical definition of the desired quantity. A generic instrument to measure the scatterance has to sample a specific volume which is illuminated by a beam of light and must have a detector that can detect the scattered light at various angles.

A. Measurement of the VSF

By definition of the backscattering coefficient in Eq. (2.13) it is obvious that by knowing the full volume scattering function one can easily calculate the backscattering

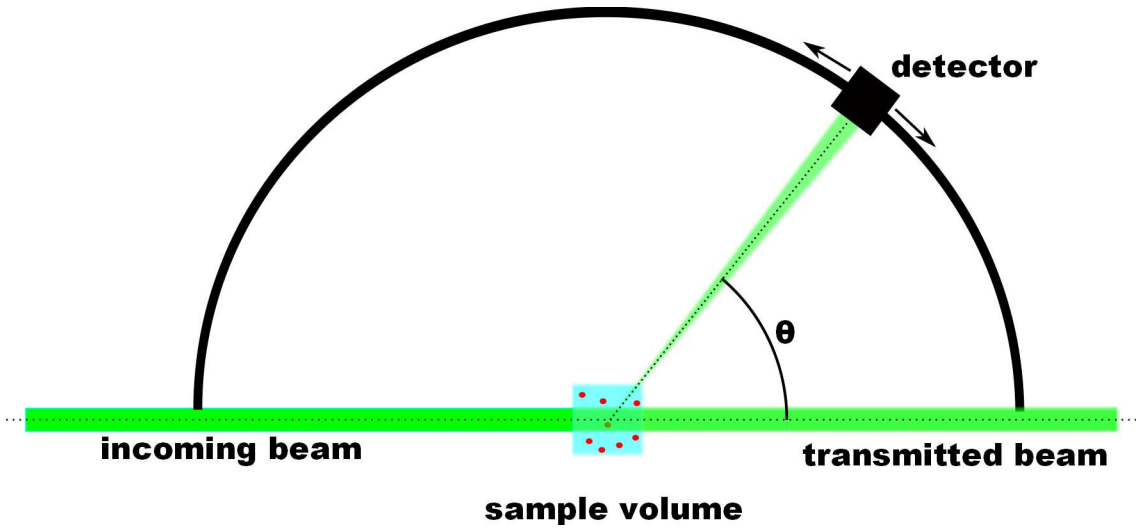

Fig. 4. Generic design for a volume scattering meter

coefficient by a simple integration.

Fig. 4 shows the generic design of a volume scattering function meter. A well defined sample volume is illuminated by a collimated light beam. A detector, with a field of view restricted to the sample volume, is mounted such that it can be moved around the sample cell and can measure the scattered signal at different angles.

A precise measurement of the VSF over the full angular range is subject to some difficulties. At very small angles, it is difficult to separate the scattered light from the incident beam. At large angles in the backward direction it is difficult to take a measurement without the detector blocking the incident beam. Additionally, the shape of the volume scattering function requires a large dynamic range of the detector, spanning multiple orders of magnitude. First measurements of the VSF *in situ* were made over 25 years ago, by, among others, Tyler and Richardson [5], Petzold [7], and Kullenberg [6]; however, operation of these instruments was difficult and the angular resolution was not satisfactory to solve the radiative transfer equation. Another problem inherent to all VSF meters is the necessity to have a small sampling volume

in order to have high resolution. If the natural water to be measured contains large particles, such as marine snow, for example, these large particles typically occur in concentrations of less than 1 particle per cm^3 and thus may not be correctly accounted for in this type of VSF measurements; however, in large scale observations, these particles can greatly affect the distribution of the light.

An improved volume scattering meter design was presented by Lee and Lewis [27] in 2003. By virtue of their design, the problems of measuring very small and large angles are largely overcome. In fact, Lee and Lewis claim to be able to measure the volume scattering function in a range from 0.6° to 177.3° at an angular resolution of 0.3°. From these measurements Lee and Lewis are able to calculate the total, forward, and backscattering coefficients, respectively. From a controlled laboratory experiment using a solution with known VSF, Lee and Lewis estimate their error in determining the backscattering coefficient b_b to be less than -8%. This error was calculated by comparing the theoretical value for b_b with the value obtained by integrating over the measured range only.

B. Cavity Approach

One of the first groups to use the integrated cavity approach was Bricaud *et al.* [28] in 1983 who reported the use of an integrating sphere to measure the backscattering coefficient of phytoplankton. Their basic laboratory design is shown in Fig. 5. A beam of light passes through a small opening into the integrating sphere, which has inside walls coated with a highly reflective material, typically with reflectivity over 99%. The light passes through this hole and the entire cavity before entering the cell containing the water sample. With the exception of the wall facing the cavity, the walls of the sample cell are coated to act as light trap, to prevent light from reentering

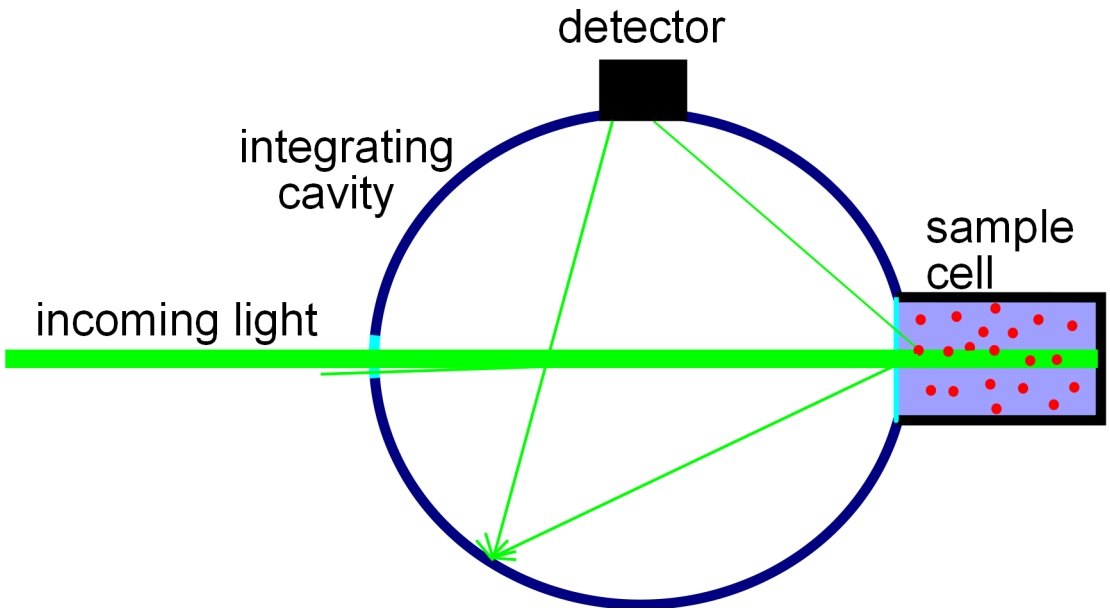

Fig. 5. Typical design for integrating sphere backscattering meter

the sample. The backscattered light is reintroduced into the cavity and potentially scattered around it before hitting a detector mounted against the sphere.

There are several problems with this design:

- Signal close to 180° cannot be collected

  Due to the necessity of getting the light into the cavity, an opening has to be created directly across from the sample cell. A certain amount of the backscattered signal close to 180° will therefore escape the integrating cavity and thus avoid detection

- Total internal reflections in the sample cell for scattering angles near 90°. Backscattered light near 90° will not make it into the cavity and therefore will not be detected

- Backscattered light can be reflected in the sphere and be reintroduced into the sample cell

- Any absorption in the integrating sphere will lead to problems since there is a range of "preferred" angles, which the light can travel from the sample cell to the detector without hitting the walls of the integrating cavity

- Reflection off the front face of the sample cell

  A percentage of the incident light will be reflected and introduced into the cavity as backscattered light without having entered the sample and will thus create a background signal that can potentially be larger than the backscattered signal.

In 2005 Kim and Philpot [29] suggested an improved version of a laboratory integrating sphere backscattering meter, which used a hemispherical sample cell instead of the previously cone shaped version. They argue that their design avoids some of the aforementioned problems. Since their work was purely theoretical based on Monte Carlo simulations, a final verdict on the quality of this design is not possible at this time.

C. Fixed Angle Approach

Today the most common way to "measure" the backscattering coefficient *in situ* consists of measuring the scattering signal at one angle, namely 120°, the so called "magic" angle.

The existence of a so called "magic" angle was first suggested by Jerlov in 1953 [30]. Comparing measured and calculated values for the backscattering coefficient Jerlov noted that it seemed that the measured values of b_b were proportional to the calculated values at a particular angle, namely 45°. A generic instrument implementation of this idea is shown in Fig. 6. Over the next decades this approach was investigated further and several other values for the "magic" angle were suggested. This refinement culminated in the paper published by Oishi in 1990 [31]. Using Mie

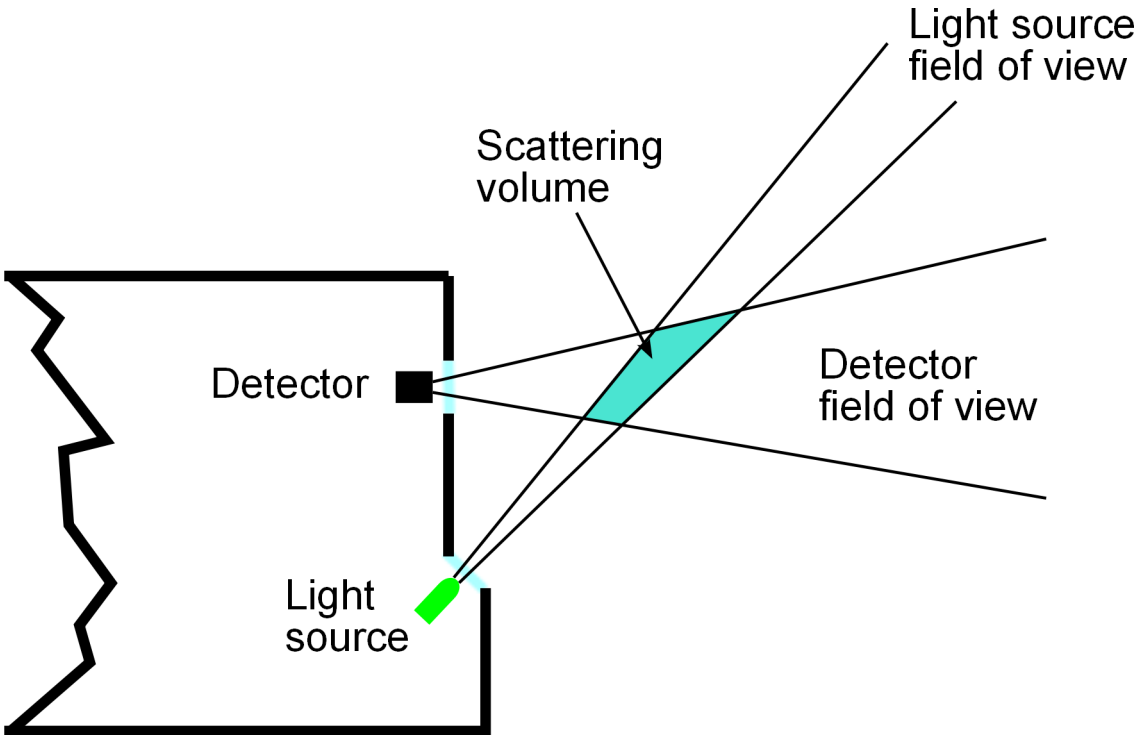

Fig. 6. Generic design of a fixed angle backscattering meter

scattering calculations, Oishi compared a multitude of different single scattering functions with size parameters ranging from 0.2 to 200 and for a variety of characteristic parameters ξ in the Junge distribution (see Eq. (2.88)). In these simulations he found that the scattering signal due to the particles at an angle of 120 °, $\beta_p(120)$, could be related to the particulate backscattering coefficient b_{bp} by

$$b_{bp} = (6.9 \pm 0.4) \times \beta_p(120). \tag{3.1}$$

Comparing the simulations to real-life data, Oishi estimated his maximum likely error to be around 17%. Further investigations were made by Maffione and Dana [32] in the mid-1990s, who compared data from some of the then available fixed angle backscattering meters. They found that there is no significant difference between using an angle of 120 °, 130 °, or 140 °. A similar result was presented by Boss and Pegau [33],

although they suggest using an angle of 117° to limit the necessary corrections to the measurement.

The main drawback of this method, however, apart from the fact that the true b_b is not measured, but extrapolated, is that while this approach is somewhat reliable as long as the measured water is within typical parameters, it will break down as soon as the volume scattering function of the water does not closely follow the Petzold phase function.

D. Inversion Algorithm

As we mentioned earlier, measurements of AOP's were performed before those of IOP's. This means that considerable work has been done on creating inversion algorithms that can calculate the absorption and scattering coefficients from irradiance measurements. As a complete discussion of the inversion problem would fill many pages, we will only briefly discuss the general theory behind this method. An example for an in-depth discussion can be found in Chapter 10 in C. Mobley's book *Water and Light* and the references therein [24].

Gordon and Boynton [34–37] and Gordon *et al.* [38] present an example of an inversion algorithm in a series of papers published between 1997 and 2009. Their algorithm takes depth profile measurements of the upward and downward irradiances, E_u and E_d, and calculates the absorption and backscattering coefficient. Gordon and Boynton estimate their errors to be about 2% for the absorption coefficient and about 10% for the backscattering coefficient. While these errors are comparable or smaller than those of the other methods, there are several drawbacks associated with it:

- As in the case of fixed-angle scattering meters, *a priori* knowledge of the VSF is required

- A relatively precise depth profile measurement of the up- and downdwelling irradiances is necessary

- The iterative algorithm takes a significant amount of time to run (in the article from 2000 [36] a running time of 16 hours is quoted), thus making any (near) real-time determination impossible

We have presented the currently available methods to determine the backscattering coefficient of natural waters. We will now present our instrument in theory and experiment and show how it avoids most of the negative aspects of the aforementioned instruments and methods.

CHAPTER IV

INSTRUMENT THEORY AND DESIGN

Consider a laser beam entering a medium at $z = 0$. The aperture to the detector that measures the scattered light is a cylindrical ring of radius R; it extends from $z = -Z_0$ to $z = +Z_0$. The laser beam is surrounded by a small tube of radius r up to the point $z = 0$ where it enters the scattering medium.

In Fig. 7 a laser beam of cross-sectional area A and irradiance E_0 enters a scattering medium along the z-axis. Consider a scattering volume of length dz and cross-sectional area A at position z. The power dP scattered at an angle θ into the detector aperture in the solid angle defined by $\theta_1 \leq \theta \leq \theta_2$ is then given by

$$dP = 2\pi A E_0 \int_{\theta_1}^{\theta_2} e^{-cx} \beta(\theta) \sin\theta d\theta dz \tag{4.1}$$

where $\beta(\theta)$ is the volume scattering function defined in Eq (2.11), c is the extinction coefficient, and x is the total distance a scattered photon travels in the medium, i.e. from $z = 0$ to the scattering volume dz and then back to the detector. The total power scattered into the detector is obtained by adding (integrating) the power dP from all elements dz,

$$P = 2\pi A E_0 \int_0^{\infty} dz \int_{\theta_1}^{\theta_2} e^{-cx} \beta(\theta) \sin\theta d\theta. \tag{4.2}$$

We will discuss the theory in two steps. At first we will look at the special case of small extinction, i.e. $e^{-cx} \approx 1$, before looking at those situations where we have to take the extinction factor into account. This two-tiered approach has several benefits, the major one being that the small extinction case allows an in-depth understanding of the theory of the instrument without the need for any further approximations,

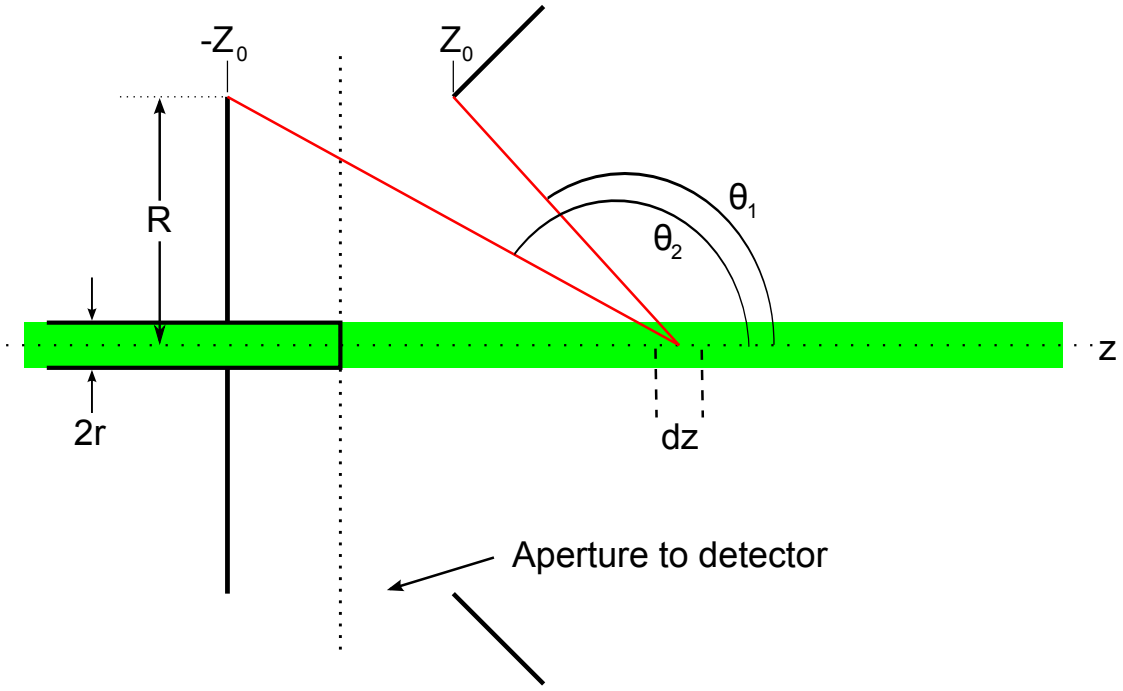

Fig. 7. Conceptual sketch of instrument

while the rigorous treatment will then give full disclosure of the limitations of this design.

A. Small Extinction

From Figure 7, we can express θ_1 in terms of z:

$$\tan(\pi - \theta_1) = \frac{R}{z - Z_0}$$
$$\Rightarrow \theta_1 = \pi - \tan^{-1}\left(\frac{R}{z - Z_0}\right). \tag{4.3}$$

And, similarly we find for θ_2

$$\theta_2 = \pi - \tan^{-1}\left(\frac{R}{z + Z_0}\right). \tag{4.4}$$

We emphasize that for a fixed value of z, the detector only observes light that is

scattered at angles θ defined by $\theta_1 \leq \theta \leq \theta_2$, where θ_1 and θ_2 are given by Eqs. (4.3) and (4.4), respectively. For a fixed value of θ, scattered light is only observed from points z between z_1 and z_2. The latter are obtained by inverting Eqs.(4.3) and (4.4):

$$\begin{aligned}
\theta_1 &= \pi - \tan^{-1}\left(\frac{R}{z - Z_0}\right) \\
z &= -\frac{R}{\tan\theta_1} + Z_0 \\
\theta_2 &= \pi - \tan^{-1}\left(\frac{R}{z + Z_0}\right) \\
z &= -\frac{R}{\tan\theta_2} - Z_0 \,.
\end{aligned}$$

Thus, we find

$$z_1 = -\tfrac{R}{\tan\theta} + Z_0 \tag{4.5}$$

$$z_2 = -\tfrac{R}{\tan\theta} - Z_0 \,. \tag{4.6}$$

At $z = 0$ we have

$$\begin{aligned}
\tan\theta_1 &= \frac{R}{Z_0} && \Rightarrow \theta_{10} \equiv \tan^{-1}\left(\frac{R}{Z_0}\right) \\
\tan\theta_2 &= \frac{R}{-Z_0} && \Rightarrow \theta_{20} \equiv \tan^{-1}\left(\frac{R}{-Z_0}\right) \,.
\end{aligned}$$

To explicitly show the z-dependence, we rewrite the total power, Eq. (4.2), received by the detector,

$$P = 2\pi A E_0 \int_0^\infty dz \int_{\pi-\tan^{-1}(\frac{R}{z-Z_0})}^{\pi-\tan^{-1}(\frac{R}{z+Z_0})} \beta(\theta)\sin\theta d\theta. \tag{4.7}$$

Reversing the order of integration in Eq. (4.7), i.e. integrating over z first, gives

$$P = 2\pi AE_0 \int_{\theta_{20}}^{\pi} \beta(\theta)\sin\theta d\theta \int_{-Z_0-\frac{R}{\tan\theta}}^{Z_0-\frac{R}{\tan\theta}} dz + 2\pi AE_0 \int_{\theta_{10}}^{\theta_{20}} \beta(\theta)\sin\theta d\theta \int_{0}^{Z_0-\frac{R}{\tan\theta}} dz. \quad (4.8)$$

After completing the integrations over z, Eq. (4.8) becomes

$$P = 4\pi AE_0 Z_0 \int_{\theta_{20}}^{\pi} \beta(\theta)\sin\theta d\theta + 2\pi AE_0 \int_{\theta_{10}}^{\theta_{20}} \beta(\theta)(Z_0\sin\theta - R\cos\theta)d\theta . \quad (4.9)$$

We can expand the second term and rewrite the whole expression as four integrals (where we split the $Z_0\sin\theta$ - integral into two),

$$P = 4\pi AE_0 Z_0 \int_{\theta_{20}}^{\pi} \beta(\theta)\sin\theta d\theta + 2\pi AE_0 Z_0 \int_{\frac{\pi}{2}}^{\theta_{20}} \beta(\theta)\sin\theta d\theta + 2\pi AE_0 Z_0 \int_{\theta_{10}}^{\frac{\pi}{2}} \beta(\theta)\sin\theta d\theta - 2\pi AE_0 R \int_{\theta_{10}}^{\theta_{20}} \beta(\theta)\cos\theta d\theta . \quad (4.10)$$

A term identical to the second integral can be added and subtracted to give

$$P = 4\pi AE_0 Z_0 \int_{\theta_{20}}^{\pi} \beta(\theta)\sin\theta d\theta + 4\pi AE_0 Z_0 \int_{\frac{\pi}{2}}^{\theta_{20}} \beta(\theta)\sin\theta d\theta - 2\pi AE_0 Z_0 \int_{\frac{\pi}{2}}^{\theta_{20}} \beta(\theta)\sin\theta d\theta + 2\pi AE_0 Z_0 \int_{\theta_{10}}^{\frac{\pi}{2}} \beta(\theta)\sin\theta d\theta - 2\pi AE_0 R \int_{\theta_{10}}^{\theta_{20}} \beta(\theta)\cos\theta d\theta . \quad (4.11)$$

Finally, combining the first two integrals gives the following result for the power

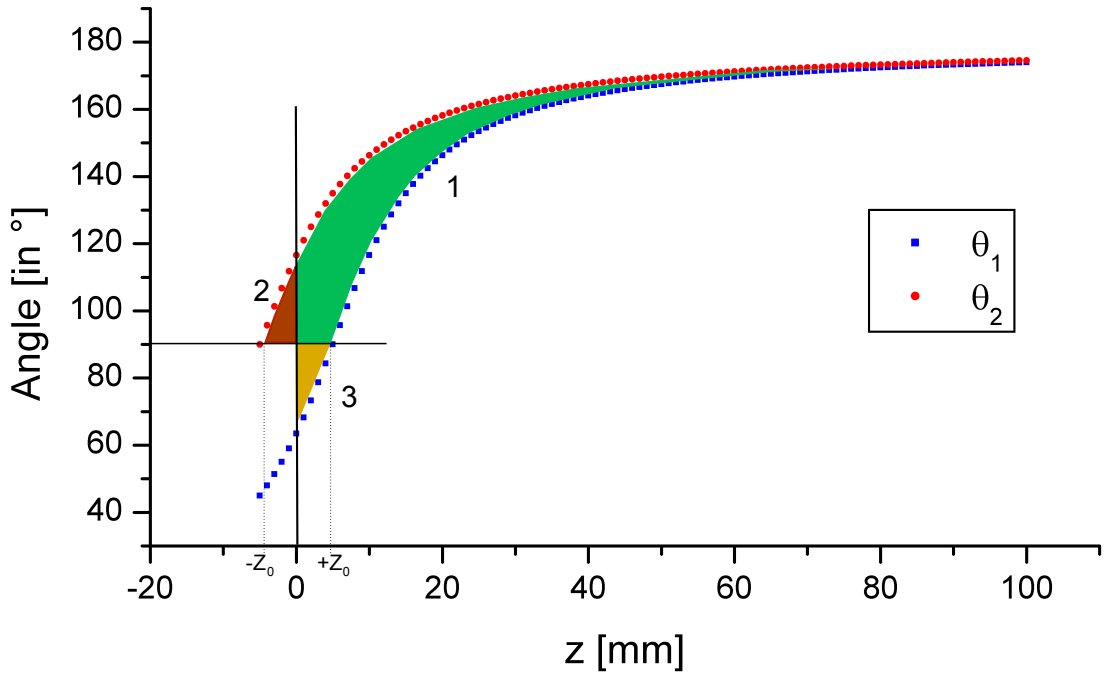

Fig. 8. The functions $\Theta_1(z)$ and $\Theta_2(z)$. Areas 1 and 2 correspond to the domain of integration of the first integral (corresponding to b_b) in Eq. (4.12)

observed by the detector.

$$P = 4\pi A E_0 Z_0 \int_{\frac{\pi}{2}}^{\pi} \beta(\theta) \sin\theta d\theta - 2\pi A E_0 Z_0 \int_{\frac{\pi}{2}}^{\theta_{20}} \beta(\theta) \sin\theta d\theta$$
$$+ 2\pi A E_0 Z_0 \int_{\theta_{10}}^{\frac{\pi}{2}} \beta(\theta) \sin\theta d\theta - 2\pi A E_0 R \int_{\theta_{10}}^{\theta_{20}} \beta(\theta) \cos\theta d\theta. \quad (4.12)$$

The first integral is, by definition, the integrated backscattering function b_b; the integration range covers Areas 1 and 2 in Fig. 8. The second integral mainly corresponds to backscattered light from the beam inside the shield that cannot reach the detector. The third integral corresponds to the small amount of forward scattered light in the range $0 \leq z \leq Z_0$ that does reach the detector. Specifically, the small

amount of light due to forward scattering that is collected (Area 3 in Fig. 8) compensates for the small amount of backscattered light that is prevented from reaching the detector due to the light shield around the laser beam (Area 2 in Fig. 8). Mathematically, $\sin\theta$ is symmetric around $\theta = 90\,^{\circ}$; consequently, if $\beta(\theta)$ is also symmetric, the second and third integrals would be identical and therefore exactly cancel. If $\beta(\theta)$ is symmetric in a small angular range around $\theta = 90\,^{\circ}$, the fourth integral would be identically zero since $\cos(\theta)$ is an odd function over the interval of integration; in addition, $\cos(\theta)$ is very small for angles around $90\,^{\circ}$, so the contribution of this integral is negligible even when $\beta(\theta)$ is not completely symmetric.

In order to demonstrate the efficacy of these symmetry assumptions, the four terms in Eq.(4.12) are numerically evaluated for a Petzold phase function. For simplicity, we denote the successive four terms in Eq. (4.12) by I, II, III, and IV, respectively. The error of interest is then

$$\epsilon = \frac{II + III + IV}{I}. \tag{4.13}$$

This error is shown in Table II for different widths of the aperture,Z_0. To summarize, $\beta(\theta)$ is not generally symmetric around $90\,^{\circ}$; but it is also not generally too asymmetric for a small angular range around $90\,^{\circ}$. To the extent that Z_0 is small and $\beta(\theta)$ is nearly symmetric, the second and third integrals in Eq. (4.12) cancel and the fourth integral is negligible. As can be seen in Table II, decreasing Z_0 reduces the contributions of the second, third, and fourth integrals. Unfortunately, this also reduces the size of the desired backscattering signal, which is also proportional to Z_0 (i.e. the first integral). Therefore, for practical applications a compromise between smallest error and largest signal has to be made.

Thus, the power which enters the detector just corresponds to the integrated

Table II. Theoretical error in the detected b_b for a Petzold VSF ($R = 1\,cm$).

Z_0 [cm]	$\frac{R}{Z_0}$	ϵ
0.1	10	0.09%
0.2	5	0.83%
0.5	2	5.81%
1.0	1	22.22%

backscattering coefficient b_b and is given by

$$P = 4\pi A E_0 Z_0 \int_{\pi/2}^{\pi} \beta(\theta) \sin\theta d\theta \quad \propto \quad b_b. \tag{4.14}$$

The detector(s) will detect a signal S which is, of course, proportional to P, so finally, we have the integrated backscattering coefficient given by

$$b_b = KS \ , \tag{4.15}$$

where K is a calibration constant which must be determined experimentally.

B. Effects of Extinction

Now let us look at the effects that extinction has on the signal and estimate the resulting error. We again start with Eq. (4.2),

$$P = 2\pi A E_0 \int_0^{\infty} dz \int_{\theta_1}^{\theta_2} e^{-cx} \beta(\theta) \sin\theta d\theta \ ,$$

but this time we will not ignore the factor for the power lost due to extinction,

$$P_{ext} \propto e^{-cx} \ , \tag{4.16}$$

where c is the extinction coefficient, the sum of scattering and absorption coefficient ($c = a + b$) and x is the total distance that the light travels through the medium. From our geometry we get

$$x = z + \frac{R}{\sin\theta} \tag{4.17}$$

and therefore Eq. (4.2) becomes

$$P = 2\pi A E_0 \int_0^{\infty} \int_{\theta_1}^{\theta_2} e^{-c(z+\frac{R}{\cos\theta})} \beta(\theta) \sin\theta dz d\theta. \tag{4.18}$$

which we write in the same way as Eq.(4.8):

$$P = 2\pi A E_0 \int_{\theta_{20}}^{\pi} \beta(\theta) \sin\theta d\theta \int_{-Z_0-\frac{R}{\tan\theta}}^{Z_0-\frac{R}{\tan\theta}} e^{-c(z+\frac{R}{\sin\theta})} dz$$
$$+ 2\pi A E_0 \int_{\theta_{10}}^{\theta_{20}} \beta(\theta) \sin\theta d\theta \int_{0}^{Z_0-\frac{R}{\tan\theta}} e^{-c(z+\frac{R}{\sin\theta})} dz. \tag{4.19}$$

Looking at the z integration we get in the first integral

$$\int_{-Z_0-\frac{R}{\tan\theta}}^{Z_0-\frac{R}{\tan\theta}} e^{-c\left(z+\frac{R}{\sin\theta}\right)} dz = e^{-\frac{cR}{\sin\theta}} \int_{-Z_0-\frac{R}{\tan\theta}}^{Z_0-\frac{R}{\tan\theta}} e^{-cz}$$
$$= \frac{1}{c} e^{-\frac{cR}{\sin\theta}(1-\cos\theta)} \left(e^{cZ_0} - e^{-cZ_0}\right) , \tag{4.20}$$

and in the second integral

$$\int_{0}^{Z_0-\frac{R}{\tan\theta}} e^{-c(z+\frac{R}{\sin\theta})} dz = e^{-\frac{cR}{\sin\theta}} \int_{0}^{Z_0-\frac{R}{\tan\theta}} e^{-cz} dz$$
$$= \frac{1}{c} \left(e^{-\frac{cR}{\sin\theta}} - e^{-cR\frac{1-\cos\theta}{\sin\theta} - cZ_0}\right) . \tag{4.21}$$

Plugging this into Eq. (4.19) we get

$$P = \frac{2\pi AE_0}{c}\left(e^{cZ_0} - e^{-cZ_0}\right)\int_{\theta_{20}}^{\pi}\beta(\theta)\sin\theta\cdot e^{-cR\frac{1-\cos\theta}{\sin\theta}}d\theta + \frac{2\pi AE_0}{c}\int_{\theta_{10}}^{\theta_{20}}\beta(\theta)\sin\theta\left(e^{-\frac{cR}{\sin\theta}} - e^{-cR\frac{1-\cos\theta}{\sin\theta}-cZ_0}\right)d\theta. \quad (4.22)$$

Splitting the second integral into two, we can write this as

$$P = \frac{2\pi AE_0}{c}\left(e^{cZ_0} - e^{-cZ_0}\right)\int_{\theta_{20}}^{\pi}\beta(\theta)\sin\theta\cdot e^{-cR\frac{1-\cos\theta}{\sin\theta}}d\theta + \frac{2\pi AE_0}{c}\int_{\theta_{10}}^{\theta_{20}}\beta(\theta)\sin\theta e^{-\frac{cR}{\sin\theta}}d\theta - \frac{2\pi AE_0}{c}\int_{\theta_{10}}^{\theta_{20}}\beta(\theta)\sin\theta e^{-cR\frac{1-\cos\theta}{\sin\theta}-cZ_0}d\theta. \quad (4.23)$$

Adding and subtracting the integral

$$\frac{2\pi AE_0}{c}e^{cZ}\int_{\frac{\pi}{2}}^{\theta_{20}}\beta(\theta)\sin\theta\cdot e^{-cR\frac{1-\cos\theta}{\sin\theta}}d\theta \quad (4.24)$$

to the expression on the right hand side of Eq. (4.23) and then combining terms gives

$$P = \frac{2\pi AE_0}{c}\left(e^{cZ_0} - e^{-cZ_0}\right)\int_{\frac{\pi}{2}}^{\pi}\beta(\theta)\sin\theta e^{-cR\frac{1-\cos\theta}{\sin\theta}}d\theta + \frac{2\pi AE_0}{c}\int_{\theta_{10}}^{\theta_{20}}\beta(\theta)\sin\theta e^{-\frac{cR}{\sin\theta}}d\theta - \frac{2\pi AE_0}{c}e^{-cZ_0}\int_{\theta_{10}}^{\frac{\pi}{2}}\beta(\theta)\sin\theta e^{-cR\frac{1-\cos\theta}{\sin\theta}}d\theta - \frac{2\pi AE_0}{c}e^{cZ_0}\int_{\frac{\pi}{2}}^{\theta_{20}}\beta(\theta)\sin\theta e^{-cR\frac{1-\cos\theta}{\sin\theta}}d\theta. \quad (4.25)$$

Label the first of these integrals P_0 and the sum of the other three integrals P_1. Note that up to this point there are no approximations in the integrals of Eq. (4.25).

Now consider P_1. Typically, R and Z_0 are 1 cm or less, so even for $c \approx 10\,m^{-1}$,

cR and cZ_0 are small. Also, throughout the integration range of all three integrals, θ is close to $\frac{\pi}{2}$ and we therefore have $\sin\theta \approx 1$. Consequently, the exponentials can be expanded in a power series giving

$$P_1 = -2\pi AE_0 Z_0 \int_{\frac{\pi}{2}}^{\theta_{20}} d\theta + 2\pi AE_0 Z_0 \int_{\theta_{10}}^{\frac{\pi}{2}} \beta(\theta)\sin\theta d\theta - 2\pi AE_0 R \int_{\theta_{10}}^{\theta_{20}} \beta(\theta)\cos\theta d\theta$$
$$+ 2\pi AE_0 \Bigg\{ cRZ_0 \int_{\frac{\pi}{2}}^{\theta_{20}} \beta(\theta)(1-\cos\theta)\, d\theta - cRZ_0 \int_{\theta_{10}}^{\frac{\pi}{2}} \beta(\theta)(1-\cos\theta)\, d\theta$$
$$- \frac{cZ_0^2}{2} \int_{\theta_{10}}^{\theta_{20}} \beta(\theta)\sin\theta d\theta + cR^2 \int_{\theta_{10}}^{\theta_{20}} \beta(\theta)\frac{\cos\theta}{\sin\theta} d\theta - \frac{cR^2}{2} \int_{\theta_{10}}^{\theta_{20}} \beta(\theta)\frac{\cos\theta^2}{\sin\theta} d\theta \Bigg\} + K \quad (4.26)$$

where the higher order terms are proportional to $c^{j+k-1}R^j Z_0^k$ with j and k ranging over all positive integers and zero, but with $j+k = 3, 4, 5, \ldots$ for successively higher orders (the terms with $j+k=1$ and $j+k=2$ are shown in Eq. (4.26)). Note first that the constant terms (i.e. those proportional to R^1 or Z_0^1) are the first three integrals in Eq. (4.26); they are identical to the error terms given by the integrals II, III, and IV in Eq. (4.12) and are small based on the previous discussion. All of the second order terms ($j+k=2$) are the other integrals in Eq. (4.26) and are just a small correction on a small correction. We now consider P_0, the first integral in Eq. (4.25). Typically, Z_0 is a few mm, so even for $c \approx 10\, m^{-1}$, cZ_0 is small. Expanding the exponentials in P_1 for small cZ_0 gives

$$\left(e^{cZ_0} - e^{-cZ_0}\right) \approx 2cZ_0 + \frac{1}{3}c^3 Z_0^3 + L \quad . \quad (4.27)$$

If only the first term in this expansion is kept, P_0 becomes

$$P_0 = 4\pi AE_0 Z_0 \int_{\frac{\pi}{2}}^{\pi} \beta(\theta)\, e^{-cR\frac{1-\cos\theta}{\sin\theta}} d\theta \quad . \quad (4.28)$$

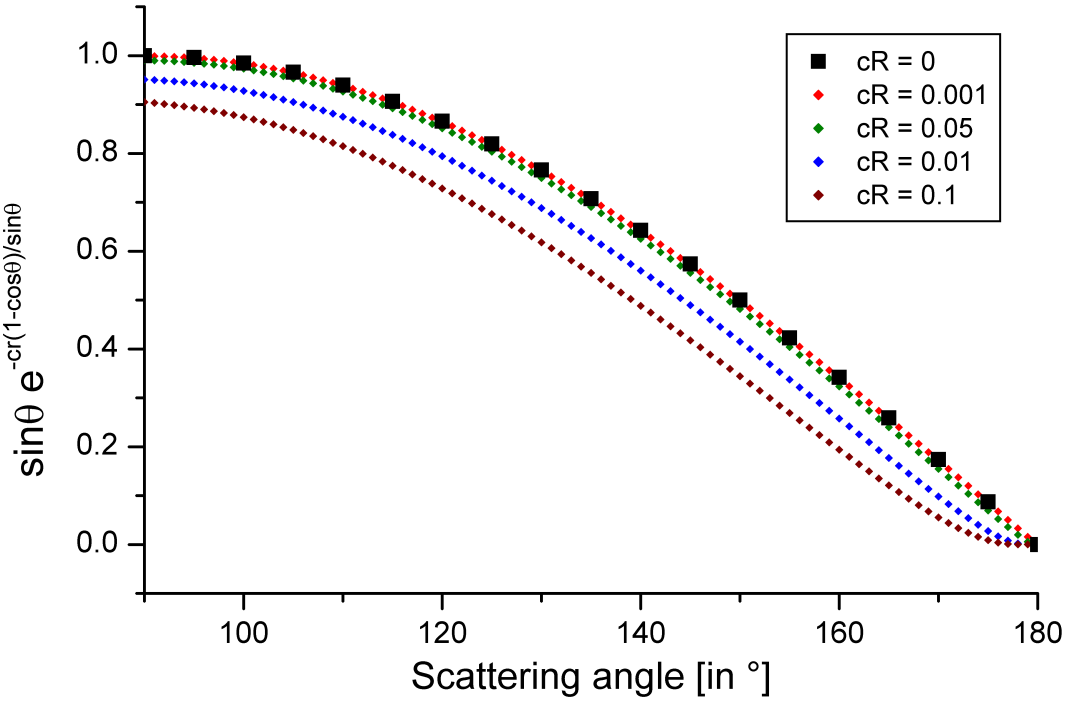

Fig. 9. Coefficient of $\beta(\theta)$ in the integrand of Eq. (4.28)

Except for the exponential function in the integrand of Eq. (4.28), P_0 is just proportional to b_b with proportionality constant $2AE_0Z_0$, i.e. b_b is explicitly defined by

$$b_b = 2\pi \int_{\frac{\pi}{2}}^{\pi} \beta(\theta) \sin\theta d\theta \quad . \tag{4.29}$$

In fact, if $c = 0\, m^{-1}$ and we set $2AE_0Z_0$ equal to 1.0, then P_0 from Eq. (4.28) is identical to b_b from Eq. (4.29). Unfortunately, the exponential function in the integrand of Eq. (4.28) cannot be simply expanded for small cR because, for $cR \neq 0$ the exponent is not always small; i.e. it is $-\infty$ at $\theta = \pi$. Nevertheless, for small cR the coefficient of $\beta(\theta)$ in the integrand is approximately $\sin\theta$ for all θ, as Fig. 9 clearly shows. In fact, on this scale, the curve for $cR = 0.001$ cannot be distinguished from the data points for $cR = 0$, the latter being just a plot of $\sin\theta$. Assuming a

reasonable value $R = 1\,cm = 0.01\,m$, the parameter cR would be only 0.01 for an extinction of $1\,m^{-1}$. Even in this case, Fig. 9 indicates that the quantity P_0 in Eq. (4.28) would be a relatively accurate measure of b_b. Of course, the quantity actually measured by the instrument is $P = P_0 + P_1$ defined in Eq. (4.26).

To further investigate the accuracy with which our b_b meter design would actually measure b_b, we consider two examples of the volume scattering function $\beta(\theta)$ that represent extreme cases - a Rayleigh phase function, and the particulate phase function given by Mobley *et al.* [39] that was based on Petzold's data. Calculations of the expected experimentally measured value of $P = P_0 + P_1$ as given by Eqs. (4.26) and (4.28) were compared with the exact value of the backscattering coefficient calculated from Eq. (4.29). For the purpose of this comparison we set the proportionality factor $2AE_0Z_0 \equiv 1$ in both P_0 and P_1 so that in the limit $c = 0$, P_0 will be identical to b_b. The percent error $(P - b_b)/b_b \cdot 100$ is plotted as a function of the extinction $c\,(m^{-1})$ in Fig. 10. At $c = 0\,m^{-1}$, the error is zero with the Rayleigh phase function regardless of the detector aperture $2Z_0$ because this phase function is symmetric around $\pi/2$; the error is non zero for the Petzold phase function and increases rapidly with increasing Z_0 because this phase function is not symmetric in a small angular range about $\pi/2$. Even so, for $Z_0 = 0.003\,m$ (width of the detector aperture $= 6\,mm$) the error is less than $\pm\,3\%$ at an extinction coefficient of $1\,m^{-1}$ for either extreme of these phase function possibilities.

It is also apparent from Fig. 10 that the percent error is almost linear in extinction. The slope is slightly greater for a Rayleigh phase function than for the Mobley phase function, but clearly one should be able to introduce an extinction-dependent factor that would provide a correction to the measurements observed with this b_b meter; such a factor could dramatically improve the accuracy at higher values of extinction. Fig. 11 presents the results using such a factor: it shows the percent

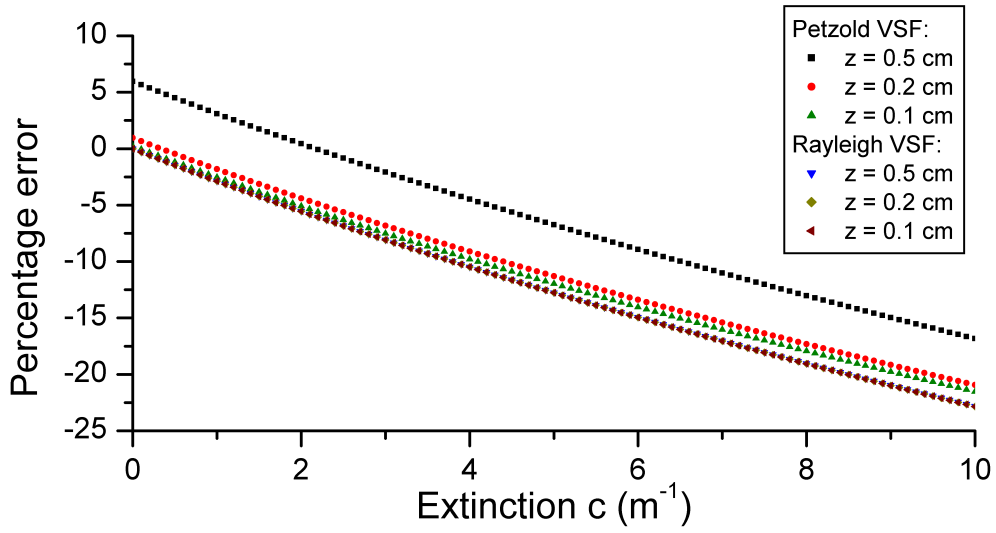

Fig. 10. Percent error with respect to the true b_b of the calculated value for P, i.e. $(P - b_b)/b_b \times 100$ is plotted as a function of the extinction $c\,(m^{-1})$

error as a function of extinction when the measured values of P are multiplied by an extinction-dependent factor to obtain a corrected P'

$$P' = (1 + 2.72cR)\,P \quad . \tag{4.30}$$

Of course, this requires an additional measurement of c, but with a detector aperture of $2Z_0 = 4\,mm$, the error in b_b would be less than $\pm\,2\%$ at $c = 5\,m^{-1}$.

C. Instrument Implementation

Fig. 12 shows a cross-section through one possible implementation for the integrated backscattering meter. Our design is approximately 30 cm in length and 15 cm in diameter. The weight is below 1 kg, excluding the detector and power supply for the laser.

The laser is integrated into the instrument, so that only a power cable and the reference and output signal fibers are taken outside the casing. While the design

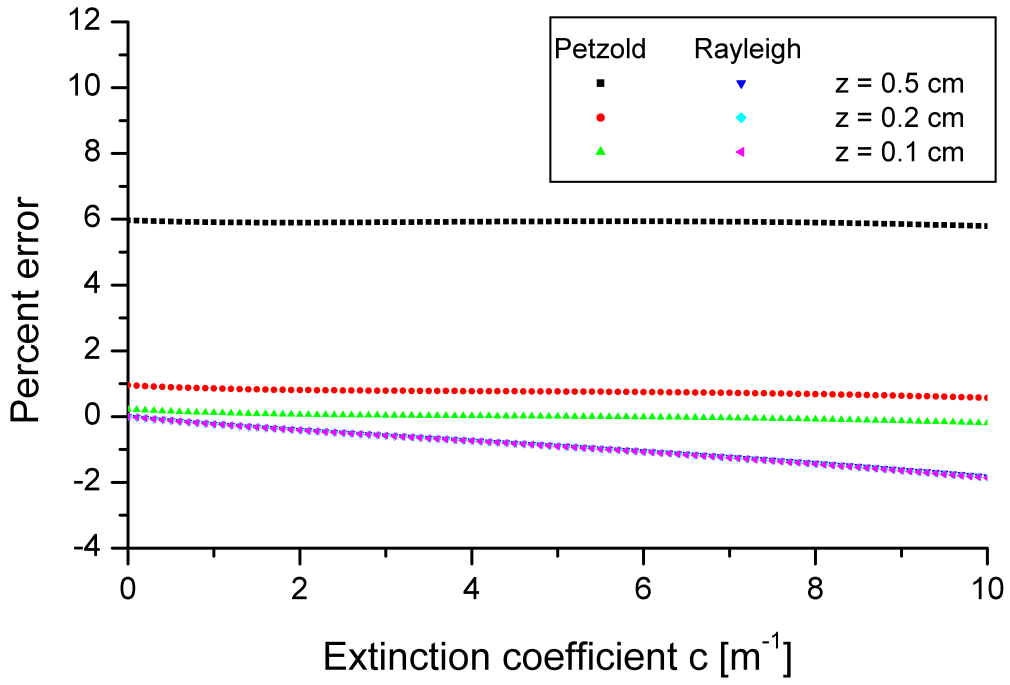

Fig. 11. Percent error with respect to the true b_b of the calculated value for P', i.e. $(P' - b_b)/b_b \times 100$ is plotted as a function of the extinction $c\,(m^{-1})$

is compact enough to be suitable for *in situ* applications, the power supply for the laser, the detectors, and the electronics necessary to record the signals were left outside the instrument. As this prototype is intended as proof-of-concept of the integrated backscattering meter, we chose values of $R = 1\ cm$ and $Z_0 = 0.5\ cm$. Instead of mounting detectors directly past the aperture, we guide the backscattered signal through an air cavity inside the instrument to six signal fibers. The cavity is enclosed by a layer of highly reflective quarz powder with a Lambertian scattering profile. This is done so the signal loses all directionality and no single scattering angle is dominating the signal. An additional fiber carries the normalization signal, which is picked up from reflections that occur inside the instrument before the light

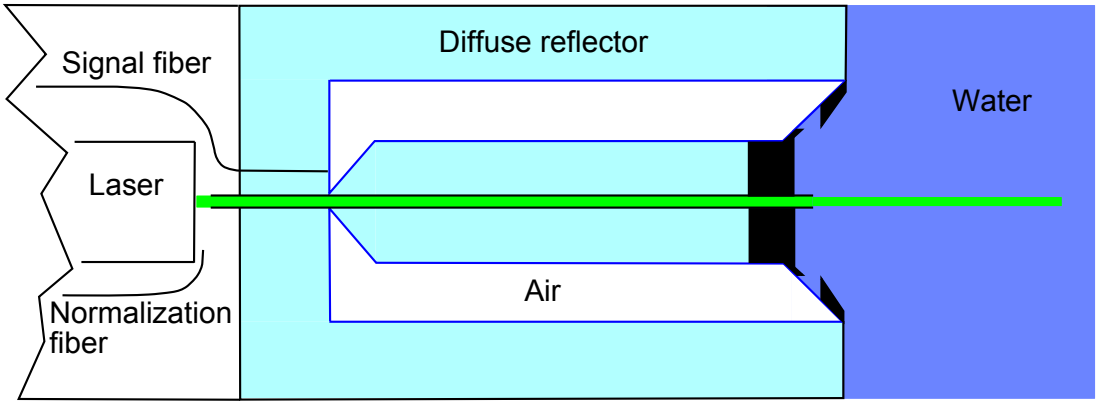

Fig. 12. Instrument implementation

is guided through a glass rod into the water.

CHAPTER V

EXPERIMENTAL SETUP

This chapter will describe the experimental setup necessary to obtain the measurements that will be presented in Chapter VI. The main components of the experimental setup as seen in Fig. 13 are: a tank to hold the water sample and the instrument (Section A); the electronic equipment to acquire the optical signal, transform it into a digital one (Section B); and a data aquisition program to evaluate and display the measured signal (Section C).

An additional measurement of the extinction in the water sample requires a separate detector and electronics. It has been omitted from Fig. 13 and will be discussed in Section D. This section will also contain a brief theoretical treatment on how to obtain the extinction coefficient from the measurements taken.

A. Water Tank

While it might seem to be a trivial matter, some thought has to be spent on the ideal design of the water tank. The biggest difficulty arises from the fact that if one wants to obtain calibration data with sufficient confidence, extremely pure water has to be used. Any contaminants in the water will affect at least one, if not both, absorption and/or scattering coefficients, meaning the tank has to be made of a material that does not contaminate the water for the duration of the experiment. It should prevent any airborne particles from getting into the water while still giving easy access to allow mixing of the PSL spheres to obtain well defined backscattering for the calibration measurements. Obviously, the tank has to be large enough to easily contain the instrument and to allow the laser beam to travel far enough such that no reflection off the far end or any side wall can make it back to the detector.

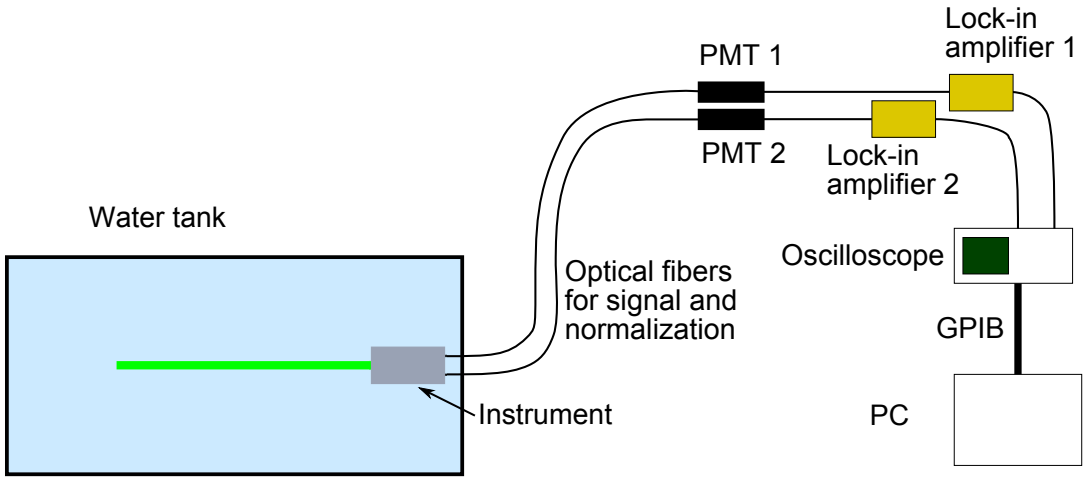

Fig. 13. Experimental setup

Our chosen tank is approximately $180\,cm \times 60\,cm \times 60\,cm$ and can hold up to 600 liters. For the calibration measurements, the tank was filled with 132 liters of high purity water that has been prepared using a Millipore water purification system with a 0.2 micron particle filter at the outlet.

B. Data Aquisition

The signal fibers run into a photo multiplier tube outside the instrument, that converts the optical signal into a electric current. This current is then fed to a lock-in amplifier that is locked to the pulse frequency of the laser beam. The laser beam is pulsed at the arbitrary, but fixed frequency of 1 kHz. The function of the lock-in amplifier is to block signals that are produced by sources other that the laser, for example, ambient light. The output of the lock-in amplifier is a DC signal proportional to the input AC signal. This DC signal is then sent to an oscilloscope, where it can be read out to a PC via the GPIB protocol. The signal may be visually monitored on the oscilloscope screen in real time.

The normalization signal is processed in the same way as the backscattered signal,

and is separately transferred to the PC.

C. Data Processing

To simplify the data processing, a program has been written to remotely control the oscilloscope and transfer the data onto the PC. Via the GPIB interface, commands are sent to the oscilloscope to set the appropriate time and signal scale. During the experiment, data is received by the PC. The program then converts this information into an easily interpretable form. The data received by the PC contains the full waveform seen on the oscilloscope. To minimize the influence of small, random variations in the signal and to increase the precision of the calibration, each data point is the average of 75 measurements, each of which in turn is the average of 10000 datapoints taken during a 400 ms interval. Each datapoint is thus the averaged signal over 5 minutes.

D. Extinction Measurements

To measure the extinction in the water tank, a small detector was built that can be moved around the tank. It measures the transmitted light from the laser up to the point where the detector is inserted into the water. A cross sectional drawing of the detector is shown in Fig. 14.

The detector is made out of a PVC pipe 5 cm in diameter and approximately 10 cm long. Sandblasted glass plates are used to diffuse the incident light as much as possible, while spectralon creates a uniform light field inside the inner cavity. This is important to decrease a dependency on where the incident beam hits the front face of the detector. The area of the exposed glass plate of the detector is approximately $5cm^2$. As neither the instrument nor the detector are fixed in the tank, this size was

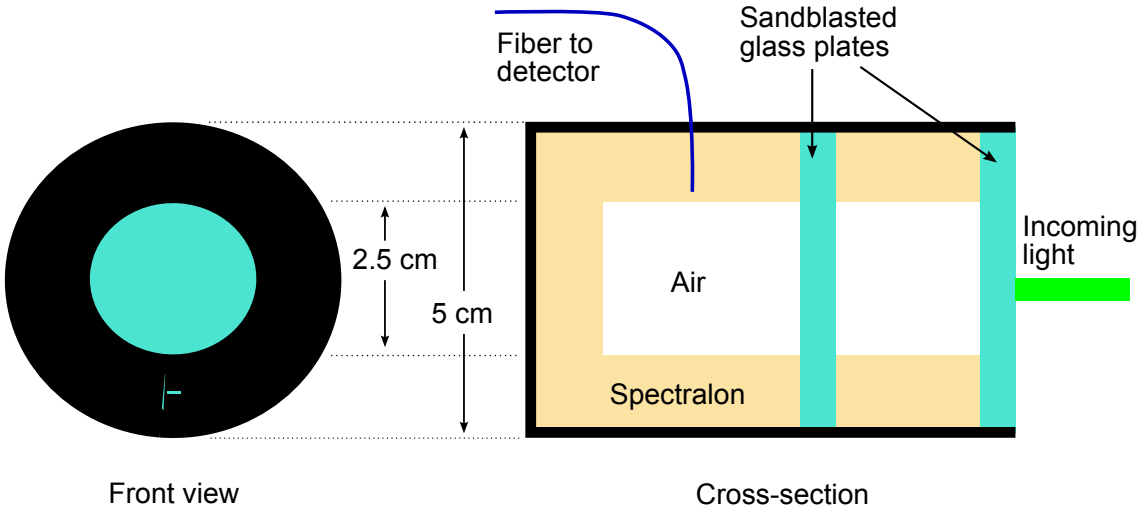

Fig. 14. Schematics of the extinction detector

chosen to ensure that the full transmitted beam is detected. Unfortunately, this also means that measurements taken with this detector will always slightly underestimate the total extinction in the tank because small angle forward scattered light will be detected and counted as transmitted light. This effect will increase with higher extinctions because the distance from the instrument, where the transmitted beam is measured, decreases and thus a larger angle of the forward scattered light is detected. Since a measure of the extinction of the water can greatly improve the accuracy of the backscattering measurement, this tradeoff was considered acceptable. A fiber carries the signal from the inner cavity to a photo multiplier tube, where the optical signal is then converted into an electronic one, which is then run to the oscilloscope after passing a lock-in amplifier, in the same manner as the backscattered signal. The brass end-cap is sealed at the back end of the detector to prevent water from entering.

The power P received by the detector due to an extinction coefficient c at a distance x follows from the exponential decrease of the power P_0 at $x = 0$:

$$P = P_0 e^{-cx} \tag{5.1}$$

To determine the extinction, the detector is moved along the beam in the tank, and the power of the transmitted light is recorded at several points. The distance between the first point and each other measuring site is measured, and the power at the first point is designated as P_0. Due to the fact that a linear fit gives the most reliable results, Eq. (5.1) is rearranged to allow for a linear fit instead of an exponential one:

$$\frac{P}{P_0} = e^{-cx} \Rightarrow \ln \frac{P}{P_0} = -cx \tag{5.2}$$

Thus we can plot $\ln P/P_0$ versus x and then get the extinction coefficent c of the current water sample from the slope of the resulting line.

CHAPTER VI

RESULTS

In this chapter we will present the experimental data obtained with our backscattering instrument. First we will discuss the potential sources of error in this experiment, followed by a discussion of the effects of extinction, before finally showing calibration data for three different volume scattering functions.

The measured power P can be decomposed into the following contributions

$$P = P_{elec} + P_{bkd} + Kb_{b\,pw} + Kb_{b\,part} + Kb_{b\,PSL} \tag{6.1}$$

where P_{elec} is the electronic noise; P_{bkd} is the (optical) background due to reflections off the tank and off the front face of the glass rod; $Kb_{b\,pw}$ is the signal from the water molecules; $Kb_{b\,PSL}$ is the signal due to the added PSL sphere; and $Kb_{b\,part}$ is the signal from any impurities in the water at the beginning of the experiment.

In order to obtain a true calibration of the instrument, we need to determine K. From Eq (6.1) we see that the last term is the only one which is being changed during the experiments. Therefore, it is straightforward to write

$$K = \frac{dP}{db_{b\,PSL}} \tag{6.2}$$

and to see that this is just the slope of the curve obtained by plotting $b_{b\,PSL}$ vs the measured signal.

A. Error Analysis

Despite the relative simplicity of the experiment, there are still a multitude of areas in which errors can be introduced. These include errors caused by: impurities in the pure water, errors in the quoted concentration of the particle samples, electronic noise

of the photo multiplier tubes and lock-in amplifiers, optical noise due to reflections off the tank and off the front face of the glass rod, and lastly, errors caused by unwanted additions to the water tank during the experiment. We can separate these errors into two groups. The first group consists of electronic and optical noise, the amount of pure water in the tank, and impurities in the pure water. These errors, which do not change over the course of one experiment, can be dealt with relatively easily, as we will show in Section 1. The second group, however, containing the errors that directly affect the measured signal, cannot as easily be accounted for because they can change over the course of each experiment and affect each data point individually.

1. Electronic and Optical Noise, and Impurities in Pure Water

The electronic background noise P_{elec} can be determined by measuring the signal with all instruments turned on except the laser. Without the light beam, all of the collected signal must come from cross-talk between the electronic equipment. The optical noise P_{bkd}, cannot be measured by simply turning on the instrument in the empty tank, because of the complication of the difference in the refractive indices between air and water, and the inherent scattering of the pure water. The optical noise can only be determined in conjunction with the signal due to the water molecules $Kb_{b\,pw}$ themselves and any additional impurities of the pure water $Kb_{b\,part}$ at the beginning of the experiment. The difference in the relative changes of the indices of refraction comes into play as the laser beam is leaving the glass rod and entering the surrounding medium and as the scattered signal is leaving the medium and hitting the front window of the detection cavity. Furthermore, there is a non-negligible, albeit small, absorption in the water, which, compared to the absorption in air, might have an effect on the measured signal. Fortunately, from Eq. (6.2) we see that all of these errors disappear in the determination of K. Plotting the normalized signal vs the

backscattering coefficient during a calibration measurement, the sum of these errors can be easily distinguished as an offset on the signal-axis.

Another contributor to the offset on the signal-axis is the backscattered signal of pure water. This signal is an integral part of the total backscattering coefficient b_b rather than a measurement error, and since it does not change over the course of the experiment, it does not play a role in the determination of the calibration constant K. Alternatively, since the theoretical value of $b_{b\,pw}$ is known, we can add this constant contribution to the backscattering coefficient to the assumed total b_b in the tank. This latter method is used in the display of the results, since it allows for an absolute calibration of our instrument.

2. Concentration Differences of the PSL Samples

In order to minimize pipetting error and the possibility of contamination, we diluted our PSL samples in a specific manner. First, we determined that, ultimately, it is irrelevant how much we dilute the samples. All that we are interested in - and must make sure of - is that every time we add a sample tube containing the PSL solution to the tank we know exactly by how much we increased the backscattering in the water. The limit is that our sample size should be small enough to not significantly change the total amount of water in the tank.

The following method takes these factors into account.

1. Determine the exact amount of water in the tank
2. Decide on the particle size and the highest backscattering coefficient $b_{b\,PSL\,max}$ to be measured
3. Decide on the number of data points N between $b_{b\,PSL} = 0\,m^{-1}$ and $b_{b\,PSL\,max}$

4. Determine amount of PSL solution needed based on $b_{b\,PSL\,max}$ in step 2
5. Pipette the total amount of PSL solution out of the original container into a beaker
6. Add an arbitrary, but rather large amount ($\sim 100\,ml$) of pure H_2O into the beaker to dilute the PSL solution
7. Pipette equal amounts ($1\,ml$) of the diluted solution into $N+1$ sample tubes
8. Repeat step 7 until the beaker contains only a small amount of diluted solution
9. Repeat steps 6 through 8 two to three times, i.e. use this small residual amount of diluted solution to further dilute and distribute it in the $N+1$ sample tubes
10. After these steps there will always be a residual amount of highly diluted solution. Equally distribute this small amount of highly diluted solution remaining in the beaker among the $N+1$ sample tubes

Our first error source is step 1, where we determine the total amount of water in the tank. To fill the tank, $4\,l$ bottles were filled with pure water, and the water was then poured into the tank. The estimated error for each filling is 2.5%, i.e. $100\,ml$. Typically, the tank was filled with $120\,l$ of water, i.e. a total of 30 bottles was necessary. Therefore, our error in the amount of water in the tank can be estimated as

$$\Delta V_{Tank} = \sqrt{30 \cdot (100\,ml)^2} \approx 547.72\,ml. \tag{6.3}$$

Our tank contains $(120 \pm 0.548)\ l$ of pure water, so we can expect an error in the determination of the backscattering coefficient of about 0.5% due to the uncertainty in the amount of the water in the tank. Potential error sources for the exact determination of the backscattering coefficient in the tank occur every time we need

to pipette, i.e. steps 5, 7 and 10. Despite a relative small inherent error in pipetting of approximately $\Delta P_{ind} = \pm 1.5\%$ per individual pipetting, over the course of an experiment with $n = 10...15$ data points this uncertainty increases to

$$\Delta P_{ind,tot} = \sqrt{n \cdot (\Delta P_{ind})^2} \approx 5\% \,. \tag{6.4}$$

The biggest contribution to the error due to pipetting is step 5, because even small deviations from the necessary amount of PSL solution in this step will have a direct influence on the whole slope which determines our calibration constant. We reduce the pipetting error by always using an appropriately sized pipette to have the minimum number of pipettings. The largest pipette available to us has a maximum volume of 1 ml and the calibration measurement with the 4.3 μm particles needs approximately 3.5 ml of PSL solution. Thus the error in the total amount of particles to be added to the tank is

$$\Delta P_{PSL,tot} = \sqrt{4 \cdot (\Delta P_{ind})^2} = 0.03 = 3\% \,, \tag{6.5}$$

since a maximum of 4 samples of the solution with the pipette are necessary. Using this method we reduced the potential error in the concentration of the PSL spheres in the tank by 40% compared to a pipetting directly into the tank from one master solution.

For the sake of completeness, we now also calculate the error $\Delta P_{PSL,var}$ between each individual sample using the dilution method.

After we complete step 10, this error is given by

$$\Delta P_{PSL,var} = \sqrt{n_1 \left(c_1 \cdot \Delta P_{ind}\right)^2 + n_2 \left(c_2 \cdot \Delta P_{ind}\right)^2 + n_3 \left(c_3 \cdot \Delta P_{ind}\right)^2} \tag{6.6}$$

where the n_i are the respective individual pipettings of the particle solution with concentration c_i. Assuming typical concentrations of $c_1 = 1/50$, $c_2 = 1/500$, and

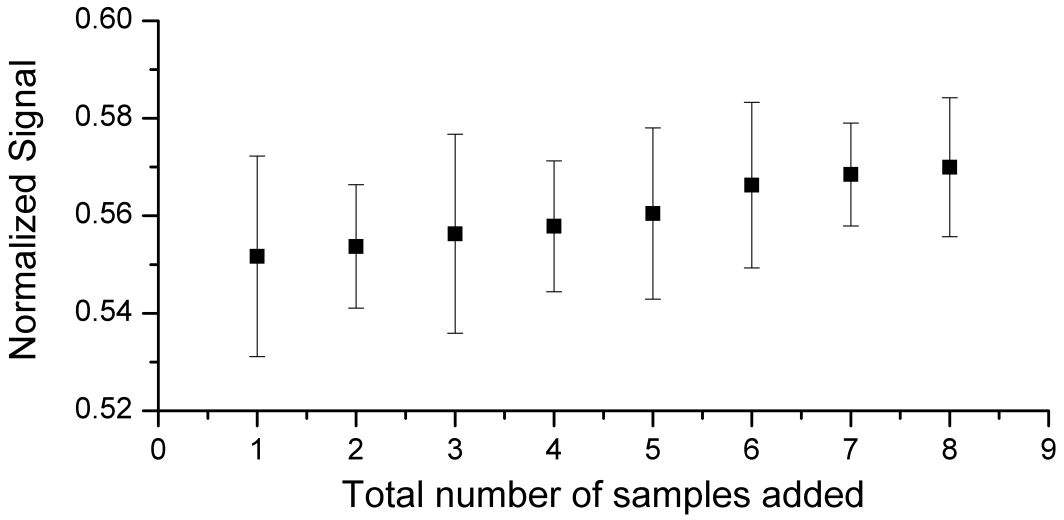

Fig. 15. Increase in b_b due to contamination of the samples

$c_3 = 1/5000$, an equal number of pipettings $n_i = 10$, and $\Delta P_{ind} = \pm 1.5\%$ as before, we get

$$\Delta P_{PSL} \approx 0.001 = 0.1\% \, . \tag{6.7}$$

This value is the variability in the amount of PSL we are adding to the tank for each data point. Any contamination that occurs after step 5 would be spread out over all data points and thus could appear as an increase in the slope of the calibration curve. If using a method of pipetting directly out of a master solution, all data points would intrinsically have significantly larger individual error bars.

It is, however, possible to estimate the influence of the pipetting in steps 5, 7, and 10 in combination with a possible contamination of the water tank during an experiment by performing a calibration experiment without particles, i.e. all steps, from the filling of the tank, dilution of the samples, and the adding and mixing of those particle-less samples into the tank are done as usual. As no particles are added to increase the backscattering coefficient, any change in signal must be caused by

unwanted contaminants. The results of this measurement are shown in Fig. 15. The data points are consistent with the expectation that there will be a small increase in the backscattering in the tank due to contamination from the individual samples. Using the calibration measurements, we can estimate that the increase per sample corresponds to an increase in the backscattering coefficient of $\Delta b_{bcont} \approx 0.00005\, m^{-1}$, or roughly $5 - 10\%$ of the backscattering coefficient of pure water. This information can be used to determine the optimum step size for the calibration measurements. In order to obtain a valid calibration, each sample should increase the backscattering coefficient in the tank significantly more than Δb_{bcont}. We deemed a minimum stepsize of $\Delta b_{b,PSL} = 0.005\, m^{-1}$, i.e. an error of $\leq 1\%$ acceptable.

3. Machining and Construction Errors

As we have seen in Chapter IV, the instrument's ability to make precise measurements relies on the (partial) cancellation of the small portion of the detected forward scattered light combined with the not-detected backward scattered light. If the glass rod that carries the laser beam out of the instrument is not exactly centered on the aperture, there could be a dependence on the shape of the volume scattering function different than anticipated, since the forward and backward scattered portions do not cancel as expected from Eq. (4.12). While the influence of the shape of the VSF on the calibration can be minimized by choosing a small aperture, as discussed in Chapter IV, potential errors in machining and assembling the instrument cannot be ignored. A silica based marine sealant was used to seal the glass and metal pieces together. This sealant takes 24 hours to set, so there is the possibility of the pieces becoming slightly offset, leading to a mis-centered glass rod with respect to the aperture. Assuming a variation of $\Delta P_{rod} = \pm 0.5\, mm$ in fixing the the rod in its desired place and an imprecision in machining the parts of $\Delta P_{mach} = \pm 0.001\, in = \pm 0.0254\, mm$ we can

ignore the latter and take ΔP_{rod} as the error in the construction of the instrument.

4. Other Potential Sources of Error

There are several other potential sources for error that we should mention, although we will not discuss them in detail since they are either outside of our control or are difficult to quantify and thus there are limited options to handle them.

Every effort has been made to avoid any influence on the signal from reflections off the walls of the tank: it has been lined with light-absorbing material and it is as large as is practical for the laboratory experiment. Its size does increase the chance of water contamination, since a larger tank takes longer to fill, and there is a larger surface area exposed to the air. We saw no evidence of such influence, but it cannot be completely ruled out.

Another variable in our calibration is the mean diameter and the size distribution of the PSL spheres. Both of these parameters play a crucial role in determining the necessary amount of PSL solution to be added to the tank. A small deviation from the reported value in either one of these numbers can have a large influence on the outcome of the measurement.

B. Absorption Effects

In order to investigate the effects of absorption on the signal, several measurements were taken at a set backscattering coefficient while the absorption was increased. The backscattering coefficient was chosen arbitrarily on the order of $b_b = 0.01\, m^{-1}$, such that small amounts of contaminants invariably introduced to the water sample during the duration of the experiment did not make a noticeable difference in the backscattered signal. Along with the initial backscattering signal, the extinction in

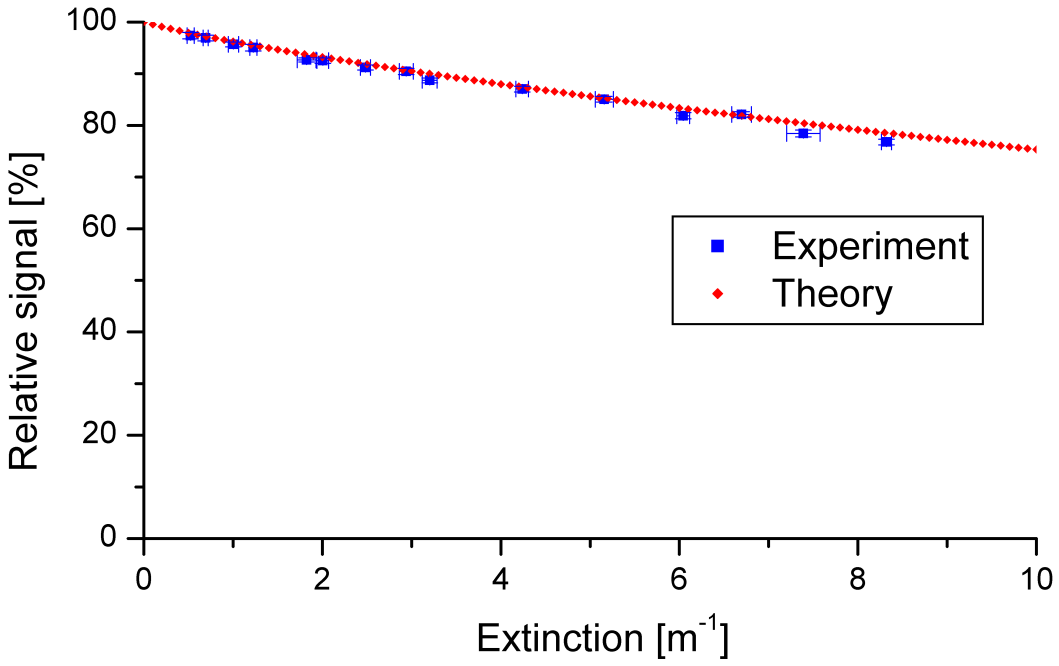

Fig. 16. Absorption effects on the measured signal

the tank was measured using the method described in Chapter V, Section D. A small amount of dye was added to the tank and thoroughly mixed in, after which new measurements of b_b and c were conducted. This was repeated until an extinction of approximately $c = 8\ m^{-1}$ was reached, which is the limit that our extinction measurements could reliably determine.

The results of one representative measurement, shown in Fig. 16, are consistent with our expectations, since, as discussed in Chapter V Section D, our detector will slightly underestimate the total extinction. Based on this measurement, we are confident that the theory presented in Chapter IV, Section B correctly describes our instrument and that the use of Eq. (4.30) to account for extinction is justified.

C. Calibration

To obtain a valid calibration, the signal was measured for particle solutions of different concentrations. First the tank was filled with a known amount of water from a Millipore water purification system that in its final stage contained a 0.2 μm filter. The signal from this water was assumed to be the signal for the backscatterring coefficient for pure water, $b_{b,pw} = 8.95 \cdot 10^{-4}\, m^{-1}$. Next, a known amount of particles was added, evenly mixed, and the corresponding signal change was recorded. The step size was chosen sufficiently large such that the unavoidable contamination discussed at the end of Section A2 did not have any noticeable influence. Since the mean particle diameter d and the width of the size distribution is known, one can use Mie calculations to obtain the backscattering efficiency Q_{back}. In addition, the amount of water in the tank V_{Tank}, as well as the volume of the particle solution $V_{PSLSolution}$ and its volume fraction f are known. We can use the equation

$$b_{b\,PSL} = \frac{3 \cdot f \cdot \frac{V_{PSLSolution}}{V_{Tank}} \cdot Q_{back}}{2 \cdot d} \tag{6.8}$$

to determine the backscattering coefficient $b_b = b_{b\,PSL} + b_{b,pw}$ in the tank.

Fig. 17 shows the results of these measurements for two different particle sizes, namely $d = 0.120\,\mu m$ and $d = 4.3\,\mu m$. Linear fits have been applied to both curves and their equations are shown in the figure. We can thus read off the slopes of the calibration curves and obtain values for the calibration constant K, as defined in Eq. (6.2), of $K_{0.120} = 56.70 \pm 0.18$ for a particle size of $d = 0.120\,\mu m$ and $K_{4.300} = 57.22 \pm 0.50$ for particles with mean diameter of $d = 4.3\,\mu m$.

Chapter IV, Section B discussed how the total extinction in the tank influences the measurement. We will now include this effect in our calibration. To minimize the possibility of contaminating the water, the extinction was only measured at the

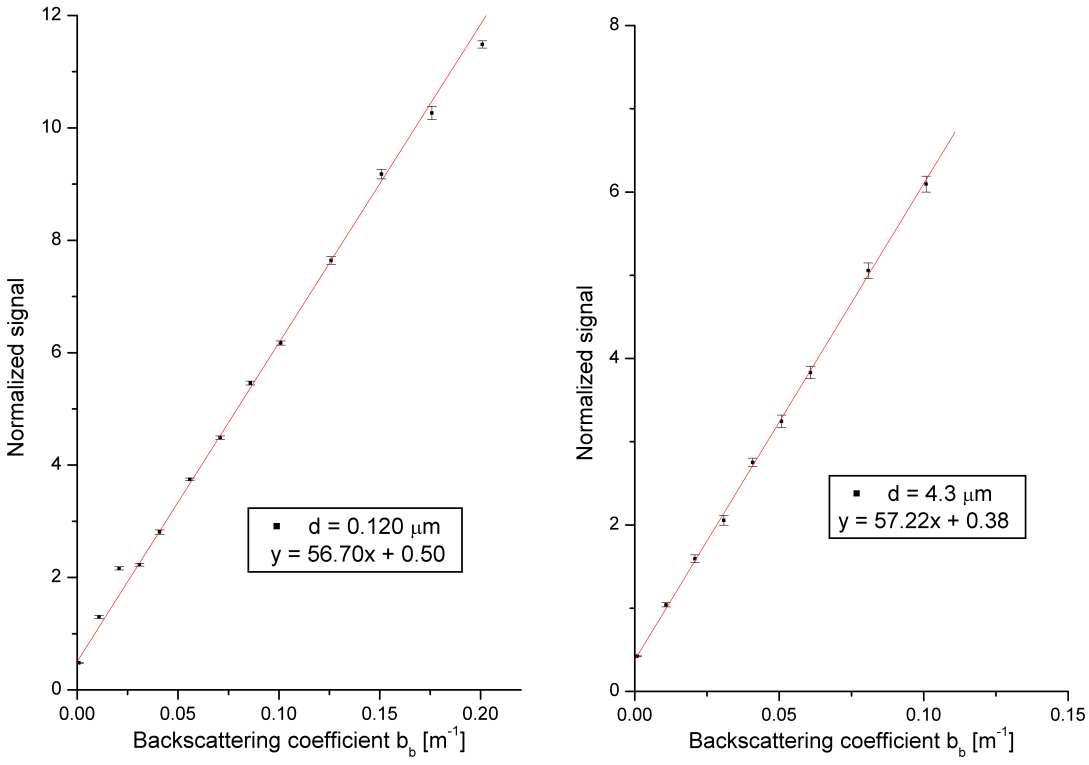

Fig. 17. Measured calibration data for particles with diameters of $d = 120\,nm$ and $d = 4.300\,nm$

beginning of each experiment, thus avoiding any unnecessary interference with the water. For all subsequent data points the only additional contribution to the extinction was assumed to come from the scattering of the added particles. The extinction in the tank was likely underestimated; however, this was deemed more acceptable than potentially adding contaminants to the tank.

In Fig. 18 a correction for extinction has been applied to the measurements and both curves have been approximated with linear fits, as before. We obtain values for

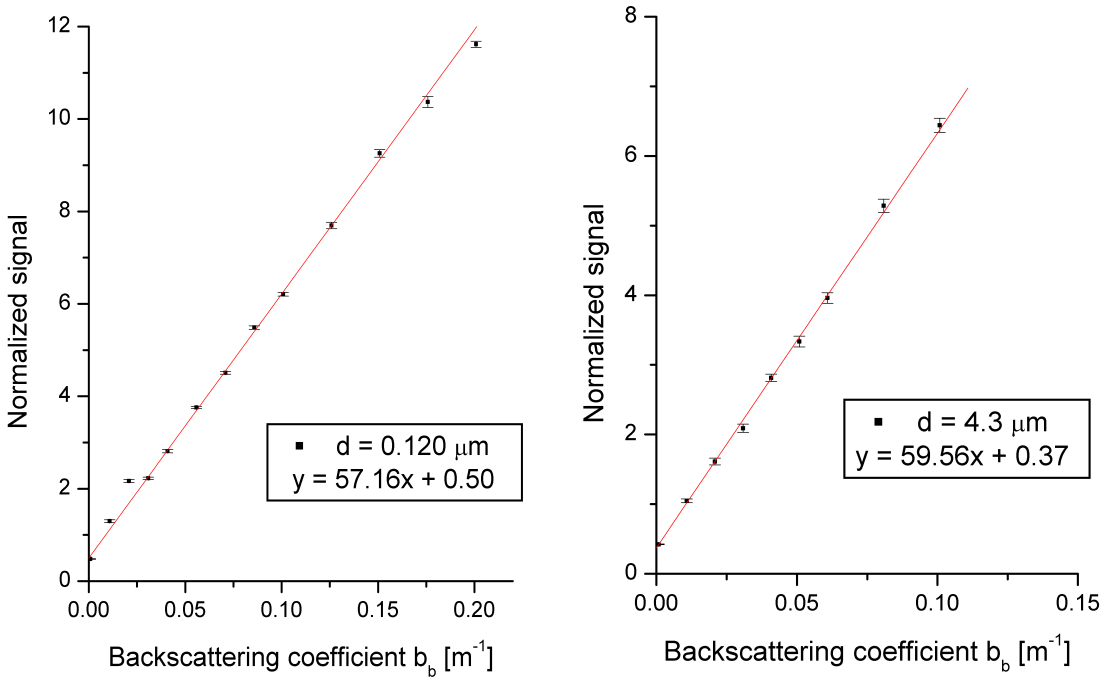

Fig. 18. Measured calibration data for particles with diameters of $d = 120\,nm$ and $d = 4.300\,nm$, correction for extinction applied

the calibration constant K of

$$K_{0.120} = \quad 57.16 \pm 0.18 \qquad (0.120\,\mu m) \tag{6.9}$$

$$K_{4.300} = \quad 59.56 \pm 0.52 \qquad (4.300\,\mu m) \tag{6.10}$$

where the error only includes the uncertainty in calculating the straight line fit. This error is quite small, thus proving that our method of preparing the individual samples discussed in Section 2 is appropriate. Including the errors discussed earlier, we get values for our calibration constant K of

$$K_{0.120} = \quad 57.16 \pm 1.63 \qquad (0.120\,\mu m) \tag{6.11}$$

$$K_{4.300} = \quad 59.56 \pm 1.77 \qquad (4.300\,\mu m) \tag{6.12}$$

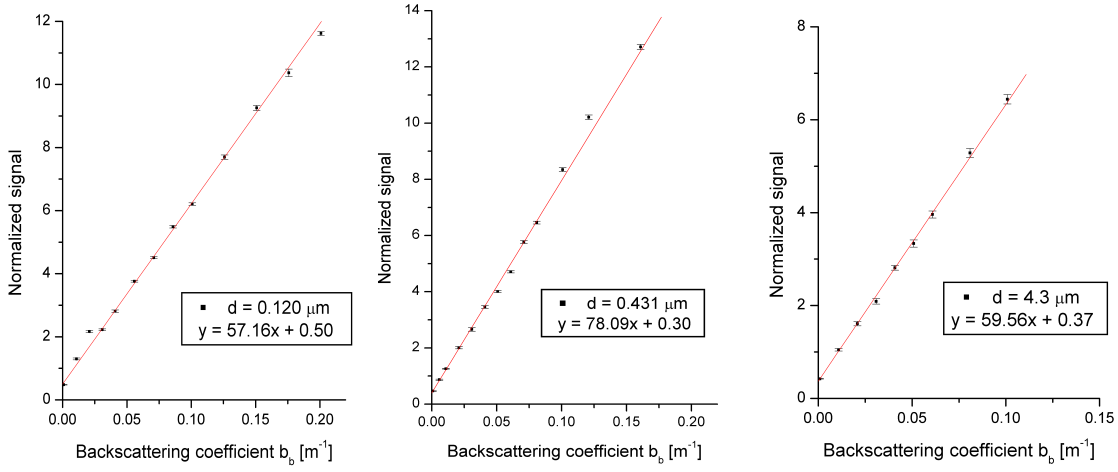

Fig. 19. Calibration data for three different VSF's, correction for extinction applied

While these values for the calibration constant are not located within each other's uncertainty, their error bars overlap. Potential reasons for this have been discussed in Section A and will not be repeated here.

To further investigate the behavior of our instrument, an additional measurement was taken using particles with a mean diameter of $d = 0.431\,\mu m$. The resulting curve of this measurement is shown in Fig. 19, along with the previous measurements. The slope of the curve for the $d = 0.431\,\mu m$ particles is distinctly different from the other two particle sizes.

The reason for this difference is the error ϵ, defined in Eq. (4.13), due to the asymmetry of the VSF. In Fig. 20 the phase functions for the used particle sizes are shown.

The symmetries in the phase functions for the $d = 0.120\,\mu m$ and $d = 4.300\,\mu m$ particles in the the area around $90\,^\circ$ are clearly visible. Equally obvious, however, is the asymmetry of the phase function for the $0.431\,\mu m$ particles in the same region. From the phase function for this particle size we can calculate the correction due

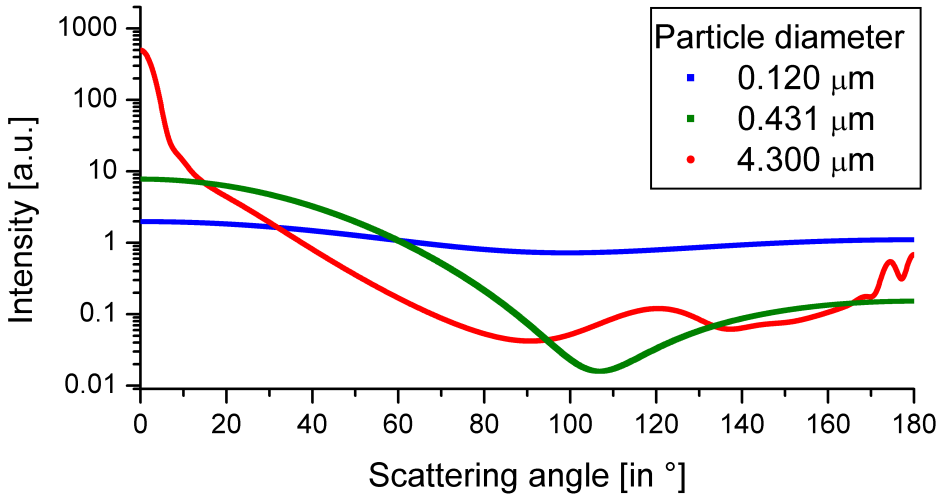

Fig. 20. VSF's for particles with mean diameters of $d = 0.120\mu m$, $d = 0.431\mu m$, and $d = 4.3\mu m$

to the asymmetry and we obtain $\epsilon_{0.431} = 139\ \%$, i.e. this is the factor that our instrument overestimates b_b in this case. Fig. 21 shows the calibration curves for all three particle sizes; the curves for particles with diameters of $d = 0.120\mu m$ and $d = 4.3\mu m$ have been corrected for extinction, and the curve for the particles with diameter $d = 0.431\mu m$ has been corrected for both extinction and asymmetry.

Comparing the adjusted slope $K^{adj}_{0.431}$ of the curve of the $d = 0.431\mu m$ particles to the previously obtained values for the calibration constant K,

$$K^{adj}_{0.431} = 56.18 \pm 1.85 \qquad (0.431\,\mu m) \tag{6.13}$$

$$K_{0.120} = 57.16 \pm 1.63 \qquad (0.120\,\mu m) \tag{6.14}$$

$$K_{4.300} = 59.56 \pm 1.77 \qquad (4.300\,\mu m) \tag{6.15}$$

we see that the adjusted slope for the $d = 0.431\mu m$ lies within the uncertainty of $K_{0.120}$, and that the error regions of $K^{adj}_{0.431}$ and $K_{4.300}$ overlap.

Based on these results we can draw several conclusions. Our experiments confirm

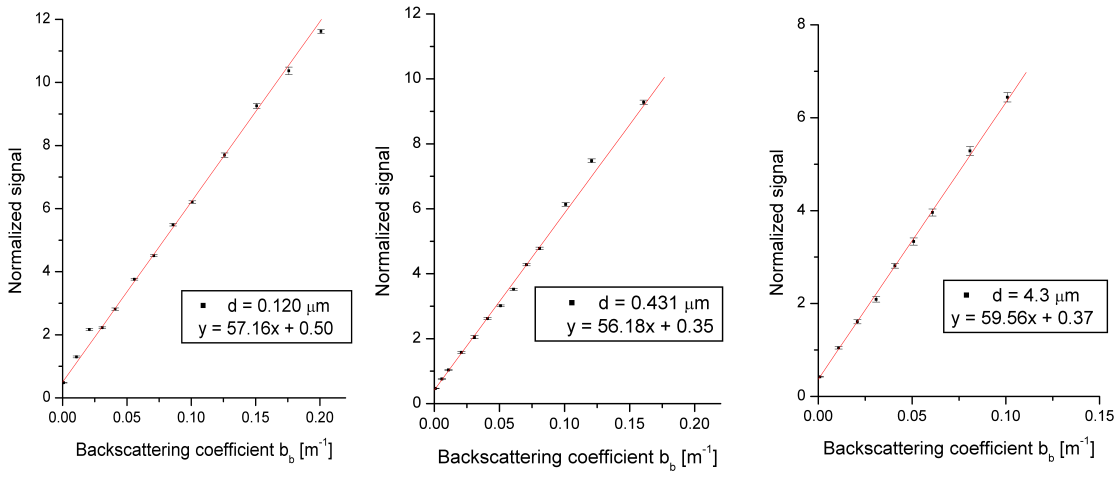

Fig. 21. Calibration data for three different VSF's, corrected for extinction (all) and asymmetry ($d = 0.431\mu m$ only)

that taking extinction into account improves the quality of our measurements, especially at higher absorptions. We have shown that the theory described in Chapter IV describes our instrument very well and that it can predict our experimental results. We have shown the proof-of-concept for a backscattering meter that avoids most of the drawbacks of other currently used methods to determine the backscattering coefficient.

CHAPTER VII

SUMMARY AND CONCLUSIONS

We have presented a novel instrument to directly measure the integrated backscattering coefficient b_b, both in theory and experiment. The theory shown explains the workings of our instrument. A calibration was obtained using particles with different volume scattering functions and confirms the accuracy of our understanding of our backscattering meter. Additionally, the effects of extinction were investigated.

We have shown that our instrument is able to accurately measure the backscattering coefficient with sufficient resolution over the full range typically occurring in natural waters.

For an improved version of our instruments several modifications should be made. Most importantly, to be capable of *in situ* operations, a fully autonomous version has to be built, since the instrument presented in this dissertation still requires laboratory-based instrumentation like photomultiplier tubes, an oscilloscope, and a PC. Another change that should be considered is to decrease the width of the aperture, as its width is the single most important factor in the precision of the determination of the backscattering coefficient for differently shaped volume scattering functions. Another potential improvement could be made through the addition of a way to measure the extinction in the water. Adding the capability to measure the backscattering coefficient at multiple wavelengths is another modification that should be considered for a second version of our instrument.

REFERENCES

[1] O. Krümmel, *Der Ozean,* vol. 52 of *Das Wissen der Gegenwart* (G. Freytag, 1886).

[2] P. A. Secchi, *Sul moto ondonso del mare* (Cialdi, 1866).

[3] L. Lorenz, "Lysbevægelse i og uden for en af plane lsybølger belyst kugle," Det Kongelige Danske Videnskabernes Selskabs Skrifter **6**, 1–63 (1890).

[4] G. Mie, "Beiträge zur Optik trüber Medien, speziell kolloidaler Metallösungen," Annalen der Physik **330**, 377–445 (1908).

[5] J. E. Tyler and W. H. Richardson, "Nephelometer for the measurement of volume scattering function *in situ*," Journal of the Optical Society of America **48**, 354–357 (1958).

[6] G. Kullenberg, "Observed and computed scattering functions," in *Optical Aspects of Oceanography*, N. G. Jerlov and E. S. Nielsen, eds. (Academic Press, 1974), pp. 25–49.

[7] T. J. Petzold, "Volume scattering functions for selected ocean waters," Tech. Rep. SIO Ref. 72-78, (Scripps Institution of Oceanography, 1972).

[8] Lord Rayleigh, "On the light from the sky, its polarization and colour (incl. appendix)," Philosophical Magazine **XLI**, 107–120, 271–279 (1871).

[9] Lord Rayleigh, "On the scattering of light by small particles," Philosophical Magazine **XLI**, 447–454 (1871).

[10] Lord Rayleigh, "On the transmission of light through an atmosphere containing small particles in suspension, and on the origin of the blue of the sky," Philosophical Magazine **XLVII**, 375–384 (1899).

[11] Lord Rayleigh, "A re-examination of the light scattered by gases in respect of polarisation. I. Experiments on the common gases," Proceedings of the Royal Society London A **97**, 435–450 (1920).

[12] J. Cabannes, "Relation entre le degré de polarisation et l'intensité de la lumiére diffusée par des molécules anisotropes. Nouvelle détermination de la constante DAvogadro," Le Journal de Physique et le Radium **6**, 129–142 (1920).

[13] R. Strutt, "The light scattered by gases: its polarization and intensity," Proceedings of the Royal Society London A **95**, 115–176 (1918).

[14] M. von Smoluchowski, "Molekular-kinetische Theorie der Opaleszenz von Gasen im kritischen Zustande, sowie einiger verwandter Erscheinungen," Annalen der Physik **330**, 205–226 (1908).

[15] A. Einstein, "Theorie der Opaleszenz von homogenen Flüssigkeiten und Flüssigkeitsgemischen in der Nähe des kritischen Zustandes," Annalen der Physik **338**, 1275–1298 (1910).

[16] L. V. King, "On the complex anisotropic molecule in relation to the dispersion and scattering of light," Proceedings of the Royal Society London A **104**, 333–357 (1923).

[17] M. Rocard, "Sur la diffusion de la lumiere dans les fluides," Comptes rendus de l' Académie des Sciences **180**, 52–53 (1925).

[18] J. Coumou, E. Mackor, and J. Hijmans, "Isotropic light-scattering in pure liquids," Transactions of the Faraday Society **60**, 1539–1547 (1964).

[19] J. Kratohvil, M. Kerker, and L. Oppenheimer, "Light scattering by pure water," Journal of Chemical Physics **43**, 914–921 (1965).

[20] G. Deželić, "Evaluation of light-scattering data of liquids from physical constants," Journal of Chemical Physics **45**, 185–191 (1966).

[21] C. F. Bohren and D. R. Huffman, *Absorption and Scattering of Light by Small Particles* (Wiley, 1983).

[22] M. I. Mishchenko, L. D. Travis, and A. A. Lacis, *Scattering, Absorption, and Emission of Light by Small Particles* (Cambridge University Press, 2002).

[23] A. Morel, "Optical properties of pure water and pure sea water," in *Optical Aspects of Oceanography*, N. G. Jerlov and E. S. Nielsen, eds. (Academic Press, 1974), pp. 1–24.

[24] C. D. Mobley, *Light and Water* (Academic Press, 1994).

[25] H. Buiteveld, J. Hakvoort, and M. Donze, "The optical properties of pure water," SPIE Ocean Optics XII **2258**, 174–183 (1994).

[26] R. M. Pope and E. S. Fry, "Absorption spectrum (380-700 nm) of pure water. II. Integrating cavity measurements," Applied Optics **36**, 8710–8723 (1997).

[27] M. E. Lee and M. R. Lewis, "A new method for the measurement of the optical volume scattering function in the upper ocean," Journal of Atmospheric and Oceanic Technology **20**, 563–571 (2003).

[28] A. Bricaud, A. Morel, and L. Prieur, "Optical efficiency factors of some phytoplankters," Limnology and Oceanography **28**, 816–832 (1983).

[29] M. Kim and W. D. Philpot, "Development of a laboratory spectral backscattering instrument: design and simulation," Applied Optics **44**, 6952–6961 (2005).

[30] N. G. Jerlov, "Particle distribution in the ocean," in *Deep Sea Expedition*, vol. 3, H. Pettersson, ed. (Swedish Natural Science Research Council, 1953), pp. 71–98.

[31] T. Oishi, "Significant relationship between the backward scattering coefficient of sea water and the scatterance at 120 °," Applied Optics **29**, 4658–4665 (1990).

[32] R. Maffione and D. Dana, "Instruments and methods for measuring the backward-scattering coefficient of ocean waters," Applied Optics **36**, 6057–6067 (1997).

[33] E. Boss and W. S. Pegau, "Relationship of light scattering at an angle in the backward direction to the backscattering coefficient," Applied Optics **40**, 5503–5507 (2001).

[34] H. R. Gordon and G. C. Boynton, "Radiance-irradiance inversion algorithm for estimating the absorption and backscattering coefficients of natural waters: homogeneous waters," Applied Optics **36**, 2636–2641 (1997).

[35] H. R. Gordon and G. C. Boynton, "Radiance-irradiance inversion algorithm for estimating the absorption and backscattering coefficients of natural waters: vertically stratified water bodies," Applied Optics **37**, 3886–3896 (1998).

[36] G. C. Boynton and H. R. Gordon, "Irradiance inversion algorithm for estimating the absorption and backscattering coefficients of natural waters: Raman-scattering effects," Applied Optics **39**, 3012–3022 (2000).

[37] G. C. Boynton and H. R. Gordon, "Irradiance inversion algorithm for estimating the absorption and backscattering coefficients of natural waters: Raman-scattering effects," Applied Optics **41**, 2224–2227 (2002).

[38] H. R. Gordon, M. R. Lewis, S. D. McLean, M. S. Twardowski, S. A. Freeman, K. J. Voss, and G. C. Boynton, "Spectra of particulate backscattering in natural waters," Optics Express **17**, 16192–16208 (2009).

[39] C. D. Mobley, B. Gentili, H. R. Gordon, Z. Jin, G. W. Kattawar, A. Morel, P. Reinersman, K. Stamnes, and R. H. Stavn, "Comparison of numerical models for computing underwater light fields," Applied Optics **32**, 7484–7504 (1993).

VITA

David Haubrich was born in 1978 in Mainz, Germany, and graduated from Theresianum, Gymnasium des Johannesbundes, with the Abitur in 1997. He attended Johannes Gutenberg-Universität Mainz where he got his B.S. in physics in 2000. He joined Texas A&M University in Fall 2001. He can be reached at Texas A&M University, Dept. of Physics, TAMU 4242, College Station, TX, 77843.